AUTONOMOUS SHIP SCHEDULING OPTIMIZATION

XIAO YANG

PhD

The Hong Kong Polytechnic University

2022

The Hong Kong Polytechnic University

Department of Electrical Engineering

Autonomous Ship Scheduling Optimization

Xiao Yang

A thesis submitted in partial fulfillment of the requirements for the degree of Doctor of Philosophy

August 2021

CERTIFICATE OF ORIGINALITY

I hereby declare that this thesis is my own work and that, to the best of my knowledge and belief, it reproduces no material previously published or written, nor material that has been accepted for the award of any other degree or diploma, except where due acknowledgement has been made in the text.

_____(Signed)

XIAO YANG (Name of student)

Abstract

The shipping industry has started to investigate and employ autonomous ships to overcome various problems that come along with the ever-increasing waterborne transport volumes, energy consumption, and seafarer shortage. This dissertation deals with two autonomous ship scheduling problems: an autonomous ship scheduling problem with a waterway bottleneck, and an autonomous vessel train scheduling problem in a hub-and-spoke network.

For the first problem, we develop a novel schedule optimization model for autonomous vessels passing a waterway bottleneck. The autonomous vessels are controlled by a central planner who enforces the optimal schedules. The model minimizes the vessel bunker cost and delay penalty at destinations by incorporating the realistic, nonlinear relationship between bunker consumption and sailing speed. The nonlinear model is linearized via two approximations. The first one linearizes the bunker consumption function using a piecewise linear lower bound, while the second does so by discretizing the time. Numerical experiments show that the discrete-time approximation model produces better solutions with lower computational costs than the continuous-time, piecewise-linear approximation, especially for large-scale problems. Numerical case studies are conducted for a real-world waterway bottleneck, the Three Gorges Dam lock. Results reveal how the optimal cost components and autonomous vessels' schedules and delays are affected by key operating parameters, including the fuel prices, delay penalty rates, and the tightness of sailing time windows. Comparison

against two simpler benchmark scheduling strategies (one with no vessel coordination and the other adopting a naïve coordination) manifests the sizeable benefit of optimal autonomous vessel scheduling.

Before resolving the technological difficulties required for a full automation, autonomous vessel train is a promising transitional solution to autonomous ship operations. A vessel train features a conventional, manned leader ship that pilots several autonomous ships (the followers) from their origin ports to destination ports. Present autonomous ships are small-sized and thus suitable for serving as feeders in a regional hub-and-spoke waterway network. We develop novel models for jointly optimizing the autonomous vessel assignment to the vessel trains, and the sequence of ports of call and the schedule of each vessel train in a hub-and-spoke network. Two mixed-integer programming models are developed, one for the freight distribution problem and the other for the vessel backhaul problem. Solutions to these models capture the optimal tradeoff between the added detour and delay costs of vessel trains and the lower sailing cost of autonomous ships. Numerical case studies are carried out for a real-world short-sea shipping network around the Bohai Bay of China. Results reveal sizeable cost savings of vessel train operations as compared to using conventional ships only. Sensitivity analyses are performed to unveil how the benefit of vessel trains is affected by key operating factors, e.g., the numbers of conventional and autonomous ships, the ratio between their costs, the maximum vessel train length, and the network topology. This study can be viewed as a first step toward real implementations of the

economically competitive and environmentally friendly autonomous freight ships via vessel trains.

Keywords: optimal ship scheduling; autonomous ships; waterway bottleneck; piecewise linear approximation; discrete-time approximation; bunker cost; vessel trains; hub-and-spoke networks

Acknowledgements

Getting a doctorate degree is a long and difficult process, but it has also been the best time of my life. After several years of studies, training, and research, I feel more confident and knowledgeable than ever before. I am grateful for the valuable guidance and support I have received from many people. I could not have completed this thesis without their support.

To begin with, I would like to express my most sincere gratitude for the constant guidance I have received from my supervisor, Dr. Weihua Gu. The genius of his mind, his rigorous attitude, and his superior writing skills have greatly benefited me. I appreciate his efforts to help me develop research topics, evaluate the contribution of my research, and improve my writing and presentation skills during my PhD. I have also received his indulgence in the pursuit of interesting research topics, despite the few results I have obtained so far. As a researcher and mentor, he is and will always be my best role model.

I would also like to express my heartfelt appreciation for my co-supervisor, Prof. Shuaian (Hans) Wang. His dedication to research greatly impresses me and inspires my passion for academic work. He provided me with valuable suggestions, which illuminated my puzzles about my research pathway. The research expertise he shared with me helped me increase my knowledge about maritime shipping. Also, I learned how to develop mathematical models, design algorithms, and compose research papers from him.

My appreciation also goes to my friends and fellows at PolyU, for the days and nights we were studying and working together, and for all the fun we had in Hong Kong. I am indebted to Qiaolin Hu, Samuel, Larry, Joy, Christine, and Ran Yan, Lingxiao Wu, Wei Zhang, Dan Zhuge, Kai Wang in the transportation groups at EE and LMS, for their sincere care and friendship. I also want to thank Shuli Liu, Jin'an Shao, Jingxu Chen, Shifu Xu, Shuai Jia, Wenhao Peng, Hao Lang, Hanxiang Zhang, Ding Zou, Fuliang Wu, Xiaowen Bi, Jiaxin Wen, Ruoheng Wang, Qirui Fan, Chuang Xu, Chao Huang, Yun Li, Chaoyun Wang, Heshou Wang, Jieming Chen, Xinsheng Yang, Wenjia Yang, etc. I enjoy and value our spontaneous and wide-ranging conversations and activities.

As a final note of thanks, I would like to acknowledge my parents. It would be impossible to express my gratitude for all the selfless love and support that they have given me.

Table of Contents

List of Tables

List of Figures

Chapter 1. Introduction

Section 1.1 presents the background of this dissertation. Section 1.2 reviews related studies in the literature. Section 1.3 provides an overview of the dissertation.

1.1. Background

Waterway (including maritime and inland waterway) transportation plays a vital role in the modern world economy. Over 80% of the international trade in goods, approximately 11.1 billion tons in 2019, is carried by waterway (UNCTAD, 2020). This number had been increasing at an average annual rate of 2.8% before the COVID-19 outbreak (WTO, 2021). The total cost of waterway transportation amounts to around 0.9 trillion USD in 2021.[1] Thus, the waterway transportation industry keeps looking for innovative technological solutions that can increase the productivity or lower the cost (Yang et al., 2019). An increasingly popular innovation of this kind is autonomous vessel (Munim, 2019). Compared to the conventional manned ships, autonomous vessels have the following advantages:

(i) A fleet of autonomous vessels can be operated and controlled in a centralized way (Chen et al., 2020). This would significantly improve the efficiency of vessel operations, e.g., when multiple vessels pass through a busy bottleneck.

[1] This number is estimated using the following facts: the global maritime trade in goods is about 15.4 trillion USD (Kalouptsidi, 2021, UNCTAD, 2021a), and the transportation cost is around 5.6% of the total trade value (UNCTAD, 2021b).

(ii) Due to the novel hull designs, increased automation, and less or no crew required, autonomous vessels have lower bunker, operation, and personnel costs (Liu et al., 2016).

(iii) By minimizing the human error, autonomous vessels are safer than conventional ones (Ahvenjärvi, 2016, Liu et al., 2016).

(iv) Thanks to the reduced bunker consumption, autonomous vessels are more environmentally friendly (Ahvenjärvi, 2016).

Thus, research institutions and industrial practitioners become increasingly interested in developing this technological solution over the last two decades (Naeem et al., 2008, Khare and Singh, 2012, Rødseth, 2017, Munim, 2019). Ongoing research and development projects include MUNIN (Burmeister and Rødseth, 2016), ReVolt (Tvete, 2022), Yara Birkeland (Kremer, 2021), etc. Studies have been devoted to various aspects of autonomous vessels, including technologies (Escario et al., 2012, Höyhtyä et al., 2017, Im et al., 2018), economic viability (Kretschmann et al., 2017, Ghaderi, 2019, Akbar et al., 2021), law and regulatory issues (Karlis, 2018, Klein et al., 2020), and human factors (Wahlström et al., 2015, Ahvenjärvi, 2016).

The first problem we examine in this dissertation is how a fleet of autonomous vessels can be optimally coordinated by a central planner to pass a common, busy waterway bottleneck with the minimum total cost. This problem is important because the rapid growth in the shipping industry has resulted in severe vessel congestion at waterway bottlenecks, including busy dams, locks, canals, and terminals. For example,

a cargo ship can wait up to 3 days at the Three Gorges Dam (TGD) on the Yangtze River during the busiest seasons (Zhao et al., 2020). Due to the demand surge in Spring 2021, the waiting times for the Neopanamax and liquefied natural gas vessels to transit the Panama Canal soared to 8–9 days (Connolly, 2021), incurring huge costs (e.g., the daily cost of a large gas carrier is $77,200; see Miller (2020)). The Suez Canal obstruction in March 2021 created a waiting time cost of $400 million per hour (LaRocco, 2021). These high waiting costs render the shipping services less appealing (Lave and DeSalvo, 1968, Laih and Sun, 2014, Laih et al., 2015, Rogers, 2018).

Improving the bottleneck's capacity is an effective way to mitigate the queues at waterway bottlenecks. However, this usually involves infrastructure expansions requiring large capital investment and long construction periods (Rusinov et al., 2021). Thus, waterway management authorities and shipping companies often prefer inexpensive and convenient congestion mitigation measures via vessel voyage rescheduling. The use of remotely-controlled autonomous vessels enables the efficient implementation of optimal vessel schedules.

Vessel voyage scheduling involves adjusting vessels' sailing speeds, which will affect the vessels' bunker cost. Note that the bunker cost constitutes 50–75% of the total operating cost of ships (Notteboom, 2006, Golias et al., 2009, Ronen, 2011), and a vessel's bunker consumption increases polynomially with the sailing speed (Wang et al., 2013). Thus, the autonomous vessel voyage scheduling optimization must consider both the schedule delay and bunker costs. A key result of the autonomous vessel

scheduling problem with bottleneck passage is that any vessel queues at the bottleneck must be eliminated at the system optimal solution (that is, when the vessel schedules can be jointly coordinated and optimized). To see why, note that if some vessels may form a queue at a bottleneck, they can be coordinated to slow down so that their departure times from the bottleneck will not be changed, while their bunker costs will be reduced due to the lower speeds. This result is similar to what was reported by the well-known road traffic bottleneck studies (e.g., Vickrey (1969); Arnott et al. (1993)).

On the other hand, researchers and practitioners generally believe that fully autonomous vessels are infeasible in the near future given the present technological limitations (Gu et al., 2020). Like autonomous cars (Van Brummelen et al., 2018), transitional solutions with limited autonomy levels have been proposed to expedite the practical use of autonomous vessels. For example, a reduced crew is still needed to assist in the ship navigation. In addition, small-sized vessels are more suitable to be autonomized due to their better maneuverability during the transitional period (Liu et al., 2016). Those smaller autonomous vessels are especially fit for providing feeder service in a hub-and-spoke network, such as inland waterways, sea-river, and short-sea transportation (Munim, 2019). Practically, those autonomous feeder vessels can form vessel trains led by a manned ship to improve the safety, security, and maneuverability (Munim, 2019).

The idea of vessel trains (also termed vessel platoons) was initiated by the project Novel IWT and Maritime Transport Concepts (NOVIMAR) funded by European Union

(Munim, 2019). The leader ship of a vessel train should be a fully manned, conventional ship with navigation, communication, and control equipment for managing the entire vessel train. Follower vessels in a train are autonomous ones with less crew onboard. This crew is responsible for emergency or occasional, difficult tasks when sailing. It can be removed as the autonomy level improves. Each follower vessel can join or leave the train freely.

By significantly reducing the difficulties in navigation, communication, and control, vessel trains make it feasible to operate autonomous ships under the present technology level. Vessel train operations can reduce the crew needed, save the operating cost, and promote the level of automation in waterway transportation. It is an ideal solution during the transitional period toward full autonomy.

On the other hand, vessel train operations raise a new scheduling problem since autonomous vessels must be dispatched together with a manned leader ship, and the leader ship must take detours to escort every autonomous member to its destination. Unfortunately, the literature on ship scheduling have also by-and-large remained silent on this research problem, as we shall see next.

1.2. Literature Review

In this section, we will review the literature on vessel scheduling problems, autonomous vessel operations and autonomous vehicle platooning.

1.2.1. Ship Scheduling

The literature on ship scheduling has grown considerably over the past decades. Various ship scheduling problems involving distinct problem setups, application scopes, model formulations, and solution approaches have been tackled (Psaraftis, 2019). Comprehensive reviews of early studies in this realm can be found in Ronen (1983), Ronen (1993), Christiansen et al. (2004), Christiansen et al. (2013), Meng et al. (2014), and Psaraftis (2019). Our focus will be on those that incorporated waterway bottlenecks and how the vessels' bunker consumption was considered.

Selected studies in recent years are summarized in Table 1.1. Most of them aimed to minimize the vessels' waiting time or the associated cost, while others maximized the shipping profit (see column 2). Though most studies examined the joint scheduling of multiple vessels (column 3), many of them assumed that the vessels sailed at a constant speed (column 4).

More importantly, to our best knowledge, no work has optimized multiple vessels' sailing speeds and schedules of passing a bottleneck for minimizing the bunker cost and the delay penalty jointly (see columns 5 and 6). Note that studies that jointly optimized ship routing and scheduling considered the effect of sailing speed on bunker consumption, but they did not examine the congestion at waterway bottlenecks (Meng et al., 2015, Zhen et al., 2016, Wen et al., 2016). On the other hand, works investigating vessel queueing at bottlenecks by-and-large overlooked the relation between sailing

speed and bunker cost (Hermans, 2014, Laih and Sun, 2014, Passchyn et al., 2016, Lalla-Ruiz et al., 2018, Deng et al., 2021). The only exception seems to be Tan et al. (2018), which developed a bi-objective program to optimize ship sailing speeds and the schedule for visiting a bottleneck. Unfortunately, that work only focused on a single ship in the interest of deriving an analytical solution.

Table 1.1. Selected studies on ship scheduling problems.

Study	Objective	Number of ships	Varying sailing speed	Bunker consumption	Bottleneck	Solution Approach
Hermans (2014)	Minimize waiting time	Single	No	No	Yes	Polynomial-time deterministic algorithm
Laih and Sun (2014)	Eliminate waiting time	Multiple	No	No	Yes	Analytical method
Meng et al. (2015)	Maximize shipping profit	Multiple	No	Yes	No	Branch-and-price
Passchyn et al. (2016)	Minimize waiting time	Multiple	No	No	Yes	Dynamic programming
Zhen et al. (2016)	Minimize bunker and transshipment cost	Multiple	Yes	Yes	No	Modified branch-and-bound
Wen et al. (2016)	Maximize shipping profit	Multiple	Yes	Yes	No	Heuristic & branch-and-price
Tan et al. (2018)	Minimize bunker consumption and ship roundtrip time	Single	Yes	Yes	Yes	Relaxed nonlinear programming and convex programming
Lalla-Ruiz et al. (2018)	Minimize waiting time	Multiple	No	No	Yes	Heuristic method
Meisel and Fagerholt (2019)	Minimize bottleneck transit time	Multiple	Yes	No	Yes	Metaheuristic method
Deng et al. (2021)	Minimize social cost	Multiple	No	No	Yes	Analytical method

Regarding the solution approach, most cited studies developed exact solutions via analytical methods, branch-and-bound approaches, or polynomial-time algorithms, while some also relied on heuristic methods (column 7).

Note that all the above-cited studies assumed conventional manned ships. The literature on autonomous ship scheduling for bottleneck passage is absent. Nevertheless, our autonomous ship scheduling problem for bottleneck passage is similar to the

problem involving conventional ships instead, if the conventional ships can also be controlled by a central planner.

We find that the effect of bottlenecks has also been extensively studied for roadway traffic. Since the seminal work of Vickrey (1969), a large collection of papers have studied variants of the Vickrey's model (e.g., de Palma et al. (1983), Arnott et al. (1990), Arnott et al. (1993), Yang and Meng (1998), Xiao and Zhang (2013), Li et al. (2017)). To their credit, the above works have unveiled important (and sometimes surprising) insights regarding the temporal pattern of congestion and optimal congestion pricing (Small, 2015). Unfortunately, their models cannot be directly applied to our autonomous ship scheduling problem with a bottleneck for various reasons. First, the roadway and waterway bottleneck models have different objectives. This is because cars carry passengers who value the travel time high, while ships often carry time-insensitive freight. In the latter case, fuel cost weights more than the value of travel time. As a result, cars prefer to travel at the free-flow speed, while ships may intentionally slow down to save fuel. Second, roadway traffic is often modeled as a continuum due to the great number of cars, while ships traveling in a waterway are not because they are sparse in space. Finally, the voyages and schedules of a group of ships can often be coordinated by a central operation manager (e.g., by the shipping company that manages a fleet, or by the manager of a dam lock). This is not the case for private vehicles, which are controlled by individual drivers.

1.2.2. Autonomous Vessel Operations

For the technical development, business models, and economical analysis of autonomous ships, one can refer to Munim (2019), Gu et al. (2020), and Ziajka-Poznańska and Montewka (2021).

Table 1.2 summarizes selected studies on autonomous vessel operations. Some works examined the operations of individual autonomous vessels instead of vessel trains; see the 2nd-4th rows of the table. They focused on either the cost-benefit analysis (Kretschmann et al., 2017) or the vessel scheduling problem (Akbar et al., 2021, Zhang and Wang, 2020). Of note, Akbar et al. (2021) modeled a hub-and-spoke shipping network similar to the one studied in the present paper. Other works investigated autonomous vessel trains mixed with conventional vessels or not; see the 5th-8th rows of Table 1.2. Unfortunately, none of these latter-cited studies has examined the optimal scheduling problem of autonomous vessel trains.

To our best knowledge, the only study that optimized the schedules of autonomous vessel trains is Chen et al. (2020); see the last row of Table 1.2. However, this study assumed that autonomous vessels and vessel trains can sail themselves without being led by manned ships. Thus, it did not consider vessel detours. Note that detours are unavoidable when autonomous vessels must be piloted by manned ships. Considering these detours will render the scheduling problem formulation more complicated.

Table 1.2. Selected studies on autonomous vessel operation problems.

Study	Objective or focus	Autonomous vessel	Vessel train	Manned vessel as leader	Vessel scheduling	Methodology
Kretschmann et al. (2017)	Autonomous ships' economic potential	Yes	No	No	No	Cost-benefit analysis
Zhang and Wang (2020)	Minimize the fuel cost and delay penalty	Yes	No	No	Yes	Mixed-integer linear programming
Akbar et al. (2021)	Minimize the operating cost	Yes	No	No	Yes	Heuristics
Chen et al. (2019)	A new platoon control approach	Yes	Yes	No	No	Dynamic model
Liang et al. (2021)	Platoon control laws	Yes	Yes	No	No	Neural dynamic model
Colling and Hekkenberg (2020)	Economic viability of vessel trains	Yes	Yes	Yes	No	Cost-benefit analysis
Meersman et al. (2020)	Economic and societal benefits of vessel trains	Yes	Yes	Yes	No	Cost-benefit analysis
Chen et al. (2020)	Minimize the passing time	Yes	Yes	No	Yes	Mixed-integer linear programming

On a side note, Zhen et al. (2018) optimized the assignment of barges to tugs and the departure time of tugs from a seaport. Despite the fact that this cited study focused on conventional ships, the barge-to-tug assignment and scheduling problem is similar to the autonomous vessel train scheduling problem. Regrettably, the transportation network examined in that study is a simple one-dimensional river. Thus, their model cannot be applied to a general hub-and-spoke network.

In summary, no work has jointly optimized the assignments of autonomous ships to vessel trains led by manned conventional ships and their schedules in a hub-and-spoke network.

1.2.3. Autonomous Vehicle Platooning

We have also reviewed related works in the realm of autonomous vehicle platooning (e.g., Han et al. (2020), Wu et al. (2021), Sala and Soriguera (2021)). Detailed reviews of vehicle platooning operations can be found in Bhoopalam et al. (2018), Zhang et al. (2020), and Lesch et al. (2021). Autonomous vehicle platoons are similar to vessel trains in that they both reduce the fuel and labor costs and that they are both potentially safer than conventional vehicles and vessels operated by humans. In addition, formations of vehicle platoons and vessel trains both involve detours. However, prevailing vehicle platoon scheduling models cannot be applied to vessel trains due the following main reasons:

(i) Operations of autonomous vehicle platoons are more flexible than autonomous vessel trains. This is because an autonomous vehicle can conveniently switch between the human-driving and the autonomous-driving modes. Thus, an autonomous car or truck can join or detach from a platoon at any time or location. On the other hand, an autonomous vessel cannot join or leave a vessel train in the middle of its voyage since the crew cannot board or alight the ship en-route (Colling and Hekkenberg, 2020).

(ii) An autonomous vessel train saves bunker thanks to the technological advancement and the removal of crew and associated facilities. On the other hand, the fuel saving of a vehicle (especially truck) platoon is mainly due to reduction of air drag, which is a function of the platoon size (Tsugawa et al., 2016).

(iii) The operating environments and constraints are different between vehicle platooning and vessel training. For example, truck drivers must follow regulations on the continuous driving hours (Goel, 2010, Goel et al., 2012, Goel, 2014).

1.3. Dissertation Overview

In light of the research gap revealed above, this dissertation presents two autonomous ship scheduling problems. The first one deals with the optimal scheduling of autonomous vessels passing a waterway bottleneck. And the second optimally solves the optimal scheduling of autonomous vessel trains in a hub-and-spoke network.

For the autonomous ship scheduling problem with a waterway bottleneck, we formulate a novel model that optimizes multiple autonomous vessels' travel schedules for passing a common bottleneck. The objective is to minimize both the bunker cost and the delay penalty at their destinations.

We propose two alternative formulations to linearize the original nonlinear model. The first program used an improved outer-approximation method, originally proposed by Wang and Meng (2012), to approximate the nonlinear bunker cost function by a piecewise linear function. The second converts the nonlinear program to a binary integer program by discretizing the time. Notably, we develop improved bounds of vessel travel times that can increase the computational efficiency for both methods (see Proposition 3 in Section 2.1.3). The computational performances of the two methods

are evaluated and compared via extensive numerical experiments. Results show that the discrete-time model can produce better solutions within less runtime than the outer-approximation model, especially for large-scale problems. This finding reveals the numerical limitation of the outer-approximation method.

Further numerical results are obtained from the TGD case study. These results unveil how different vessels' optimal schedules and delays are affected by key operating parameters, including their delay penalty rates and fuel prices. The benefit of optimal vessel scheduling is demonstrated via comparison against two simpler benchmark scheduling strategies. The first benchmark strategy assumes no coordination between vessels as each of them determines its optimal sailing schedule. The second assumes that a central operation manager determines the vessels' priority for passing the bottleneck simply by their penalty rates.

For the autonomous vessel train scheduling problem in a hub-and-spoke network, we show how to optimally form and schedule autonomous vessel trains led by conventional ships to serve as feeder services in a regional waterway transportation network. Our proposed method can be readily used during the transitional period when vessels with limited autonomy level are available.

Specifically, we formulate novel models that jointly optimize the assignment of autonomous follower ships to the conventional leader ships, the vessel trains' departure time schedules, and the sequence of ports of call for each vessel train in a hub-and-

spoke network. The objective is to minimize the total sailing cost and delay penalty of the vessels. We model two opposite operating scenarios: a freight distribution scenario where all the vessels travel from a hub port to a set of feeder ports, and a backhaul scenario where all the vessels return from the feeder ports to the hub port. The models are linearized and solved via CPLEX.

A numerical case of the major ports in the Bohai Bay of China is studied. Results unveil how much of the cost the optimally scheduled vessel train operations can save. Extensive sensitivity analyses are conducted with respect to the effects of key operating factors, including the autonomous ships' sailing cost rates, delay penalty rates, the tightness of sailing time windows, the size limit of vessel trains, and the waterway transportation network topology. These unveil useful insights into the operating conditions under which the autonomous vessel trains are beneficial. The insights have implications on the future development and commercialization of autonomous vessels.

The rest of this dissertation is organized as follows. Chapter 2 investigates the optimal scheduling of autonomous vessels passing a waterway bottleneck. Chapter 3 examines the optimal scheduling of autonomous vessel trains in a hub-and-spoke network. Conclusions and future research directions are discussed in Chapter 4.

Chapter 2. Optimal Scheduling of Autonomous Vessels Passing a Waterway Bottleneck

This chapter develops a novel schedule optimization model for autonomous vessels passing a waterway bottleneck. The model minimizes the autonomous vessel bunker cost and delay penalty at destinations by incorporating the realistic, nonlinear relationship between bunker consumption and sailing speed. The nonlinear model is linearized via two approximations. The first one linearizes the bunker consumption function using a piecewise linear lower bound, while the second does so by discretizing the time. Numerical case studies are conducted for a real-world waterway bottleneck, the Three Gorges Dam (TGD) lock. Results reveal how the optimal cost components and autonomous vessels' schedules and delays are affected by key operating parameters. Comparison against two simpler benchmark scheduling strategies (one with no vessel coordination and the other adopting a naïve coordination) manifests the sizeable benefit of optimal autonomous vessel scheduling.

Section 2.1 defines the autonomous vessel scheduling problem involving a waterway bottleneck and presents the model formulations. Section 2.2 compares the solution quality and computational efficiency of the two alternative programs. Numerical results of the TGD case study are presented in Section 2.3, including the comparison against two benchmark scheduling strategies. Section 2.4 summarizes this chapter. The notation used in this chapter is summarized in Appendix A.

2.1. Models

Section 2.1.1 introduces the problem definition and key assumptions. Section 2.1.2 presents the problem formulation. Sections 2.1.3 and 2.1.4 furnish the outer-approximation and discrete-time formulations, respectively.

2.1.1. Problem Setup and Assumptions

Consider a set of autonomous vessels, denoted by V, that can be operated and controlled in a centralized way and pass a common bottleneck in a waterway network, e.g., a dam or canal. Each autonomous vessel $v \in V$ departs its distinct origin port of call at time T_v^0 and is expected to arrive at its destination port by T_v. The travel distances from autonomous vessel v's origin port to the bottleneck (the first leg of its voyage) and from the bottleneck to the autonomous vessel's destination port (the second leg) are denoted by L_{1v} and L_{2v} (nautical miles), respectively. We assume that each autonomous vessel spends a constant transit time, ω (h), on traversing the bottleneck, and that a minimum headway between two consecutive autonomous vessel passages through the bottleneck, H (h), is required to ensure safety. An autonomous vessel that cannot pass the bottleneck immediately upon its arrival will join a queue. An autonomous vessel that arrives at its destination port later than the expected arrival time will incur a penalty.

We assume that a central operation manager seeks to minimize the total bunker consumption and late arrival penalty for all the autonomous vessels. This may occur

when all the autonomous vessels in V belong to the same shipping company. The manager determines each autonomous vessel's speed profile. The bunker consumption rate of autonomous vessel v (ton/n mile) depends on its sailing speed s (knot). In this thesis we use the bunker consumption rate function proposed by Wang and Meng (2012):

$$f_v(s) = a_v \cdot s^{b_v}, v \in V \tag{2.1}$$

where $f_v(s)$ denotes the bunker consumption per nautical mile of autonomous vessel $v \in V$; and $a_v > 0$ and $b_v > 1$ are constant coefficients.[2] Autonomous vessel v's tardiness penalty, P_v (\$), is assumed to be a linear function of its delay; i.e., $P_v(y_v) = \beta_v \cdot \max\{0, y_v - T_v\}$, where β_v (\$/h) denotes the penalty per hour of delay, and y_v the actual arrival time of v at its destination port.

We derive the following two propositions from Equation (2.1):

Proposition 1. For a fixed travel distance, an autonomous vessel's bunker consumption increases with its speed.

Proof: It follows directly from the monotonicity of Equation (2.1). □

Proposition 2. An autonomous vessel will travel at a constant speed to minimize the bunker consumption if the travel distance and time are both fixed.

[2] Equation (2.1) can be replaced with other bunker consumption functions. The outer-approximation method works as long as the function is convex, while the discrete-time model can be applied even without the convexity requirement.

Proof: It follows from the strict convexity of the bunker consumption per hour, i.e., $f_v(s) \cdot s = a_v s^{b_v+1}$. Suppose autonomous vessel v's travel distance and time are L and t, respectively. It travels at speed s_1 for δt hours and at $s_2 \neq s_1$ for $(1-\delta)t$ hours ($0 < \delta < 1$) so that $s_1 \delta t + s_2(1-\delta)t = L$. The total bunker consumption is $\big(f_v(s_1)s_1\delta + f_v(s_2)s_2(1-\delta)\big)t$. If the autonomous vessel travels at its average speed, $s_1\delta + s_2(1-\delta)$, it will cover the same distance L in the same duration t. However, it will use less fuel because the strict convexity of $f_v(s) \cdot s$ renders $f_v\big(s_1\delta + s_2(1-\delta)\big) \cdot \big(s_1\delta + s_2(1-\delta)\big)t < f_v(s_1)s_1\delta t + f_v(s_2)s_2(1-\delta)t$. □

Proposition 1 yields the following two corollaries:

Corollary 1. It is never optimal for an autonomous vessel to arrive earlier than its expected arrival time.

Proof: If an autonomous vessel arrives earlier than its expected arrival time at the optimality, it can always lower its speed to reduce the bunker consumption while still arriving on time. In this way, the total bunker and penalty cost will diminish. □

Corollary 2. Under the system-optimal scheduling strategy, it is never optimal for vessels to form a queue at the bottleneck.

Proof: If a queue is formed at the bottleneck at the optimality, the central operation manager can always coordinate the autonomous vessels to sail more slowly so that the queue is eliminated while all the autonomous vessels still pass the bottleneck at the

same times as before. Then the bunker costs would be reduced without increasing the schedule delay penalties. □

In addition, Proposition 2 indicates that, given an autonomous vessel's arrival time at the bottleneck, it will travel at a constant speed from its origin to the bottleneck. The same can be said for its travel from the bottleneck to the destination, given the departure time from the bottleneck and the arrival time at the destination. Thus, we denote x_v autonomous vessel $v \in V$'s arrival time at the bottleneck. Following the above corollaries, autonomous vessel v's cruise speeds before and after passing the bottleneck are $\frac{L_{1v}}{x_v - T_v^0}$ and $\frac{L_{2v}}{y_v - x_v - \omega}$, respectively.

The problem is therefore equivalent to finding the optimal x_v and y_v ($v \in V$) for minimizing the total bunker consumption and penalty costs. We next formulate a nonlinear program for the problem.

2.1.2. Problem Formulation

The nonlinear formulation of the autonomous vessel scheduling problem involving a bottleneck is presented as follows:

[M1]

$$\min \sum_{v \in V} \left\{ \alpha \left[L_{1v} a_v \left(\frac{L_{1v}}{x_v - T_v^0} \right)^{b_v} + L_{2v} a_v \left(\frac{L_{2v}}{y_v - x_v - \omega} \right)^{b_v} \right] + \beta_v \cdot \max\{0, y_v - T_v\} \right\} \quad (2.2a)$$

subject to

$$x_v \geq T_v^0 + \frac{L_{1v}}{s_v^{\max}}, \forall v \in V \quad (2.2b)$$

$$y_v \geq x_v + \omega + \frac{L_{2v}}{s_v^{\max}}, \forall v \in V \quad (2.2c)$$

$$\left|x_i - x_j\right| \geq H, \forall i, j \in V, i \neq j. \quad (2.2d)$$

In objective function (2.2a), the first term in the braces is the bunker consumption cost of autonomous vessel $v \in V$, where α denotes the bunker fuel price (\$/ton); and the second term is the autonomous vessel's tardiness penalty. Constraints (2.2b) and (2.2c) guarantee that an autonomous vessel's sailing speed never exceeds a maximum speed, $s_v^{\max}$ (knot). Constraints (2.2d) stipulate the minimum headway between the passages of any two autonomous vessels through the bottleneck.

Program [M1] is approximately linearized in two ways, as presented in the following sections.

2.1.3. Linearization via the Outer-approximation Method

[M1] is a nonlinear program with a nonlinear objective (2.2a) and nonlinear constraints (2.2d). Constraints (2.2d) can be linearized as follows using the Big-M method:

$$x_i - x_j \geq H + M\left(z_{ij} - 1\right), \forall i, j \in V, i \neq j \quad (2.3a)$$

$$x_i - x_j \leq -H + M z_{ij}, \forall i, j \in V, i \neq j \quad (2.3b)$$

where M is a sufficiently large number, and z_{ij}'s $(i, j \in V)$ are binary variables. The $z_{ij} = 1$ if autonomous vessel i arrives at the bottleneck after autonomous vessel j, and $= 0$ otherwise. A candidate value of M will be provided momentarily.

Next, we linearize the objective function (2.2a). First, the penalty term can be linearized by introducing a nonnegative auxiliary variable p_v ($v \in V$) that represents autonomous vessel v's delay. The penalty term in (2.2a) is then replaced with $\beta_v p_v$. In addition, the following constraints are added to the formulation:

$$p_v \geq 0, \forall v \in V \tag{2.4a}$$

$$p_v \geq y_v - T_v, \forall v \in V. \tag{2.4b}$$

Finally, we linearize the bunker fuel cost term in (2.2a) via the outer-approximation method. To this end, we first replace decision variables x_v and y_v with autonomous vessel v's travel times in the two segments, denoted by λ_v and μ_v ($v \in V$), respectively, i.e.,

$$\lambda_v = x_v - T_v^0, \forall v \in V \tag{2.5a}$$

$$\mu_v = y_v - x_v - \omega, \forall v \in V. \tag{2.5b}$$

Thus, constraints (2.2b-c), (2.3a-b), and (2.4b) are rewritten as:

$$\lambda_v \geq \lambda_v^{\min} \equiv \frac{L_{1v}}{s_v^{\max}}, \forall v \in V \tag{2.6a}$$

$$\mu_v \geq \mu_v^{\min} \equiv \frac{L_{2v}}{s_v^{\max}}, \forall v \in V \tag{2.6b}$$

$$\lambda_i - \lambda_j \geq H - \left(T_i^0 - T_j^0\right) + M\left(z_{ij} - 1\right), \forall i, j \in V, i \neq j \tag{2.6c}$$

$$\lambda_i - \lambda_j \leq -H - \left(T_i^0 - T_j^0\right) + M z_{ij}, \forall i, j \in V, i \neq j \tag{2.6d}$$

$$p_v \geq T_v^0 + \lambda_v + \omega + \mu_v - T_v, \forall v \in V. \tag{2.6e}$$

The bunker consumption in (2.2a) is now rewritten as $L_{1v} a_v \left(\frac{L_{1v}}{\lambda_v}\right)^{b_v} + L_{2v} a_v \left(\frac{L_{2v}}{\mu_v}\right)^{b_v}$. To linearize this term, we define $Q_{1v}(\lambda_v)$ and $Q_{2v}(\mu_v)$ as follows:

$$Q_{1v}(\lambda_v) = a_v \left(\frac{L_{1v}}{\lambda_v}\right)^{b_v}, \forall v \in V \tag{2.7a}$$

$$Q_{2v}(\mu_v) = a_v \left(\frac{L_{2v}}{\mu_v}\right)^{b_v}, \forall v \in V. \tag{2.7b}$$

Since $b_v > 1$, $Q_{1v}(\lambda_v)$ and $Q_{2v}(\mu_v)$ are convex functions. They are approximated by piecewise-linear, lower-bound functions denoted by $\overline{Q}_{1v}(\lambda_v)$ and $\overline{Q}_{2v}(\mu_v)$:

$$\overline{Q}_{1v}(\lambda_v) = \max\{0, \theta_{1vk}\lambda_v + \gamma_{1vk}, \forall k = 1,2,\cdots,K_{1v}\}, v \in V \tag{2.8a}$$

$$\overline{Q}_{2v}(\mu_v) = \max\{0, \theta_{2vk}\mu_v + \gamma_{2vk}, \forall k = 1,2,\cdots,K_{2v}\}, v \in V \tag{2.8b}$$

where θ_{1vk}, γ_{1vk}, θ_{2vk}, and γ_{2vk} are coefficients of the linear segments used to construct the approximate functions; and K_{1v} and K_{2v} are the numbers of linear segments. The two functions are constructed to ensure the approximation error of the total bunker cost never exceeds a predefined bound ε (\$), i.e., $\alpha \sum_{v\in V} \left|\left(L_{1v}\overline{Q}_{1v}(\lambda_v) + L_{2v}\overline{Q}_{2v}(\mu_v)\right) - \left(L_{1v}Q_{1v}(\lambda_v) + L_{2v}Q_{2v}(\mu_v)\right)\right| \leq \varepsilon$. Details on the construction of $\overline{Q}_{1v}(\lambda_v)$ and $\overline{Q}_{2v}(\mu_v)$, including the determination of coefficients θ_{1vk}, γ_{1vk} ($v \in V, k = 1,2,\dots,K_{1v}$), θ_{2vk}, and γ_{2vk} ($v \in V, k = 1,2,\dots,K_{2v}$), are relegated to Appendix B.

Built upon the above approximations, we introduce new decision variables q_{1v} and q_{2v} denoting the bunker consumption rates of autonomous vessel v's two travel segments before and after the bottleneck ($v \in V$), respectively. Then [M1] is approximated by the following mixed-integer linear program:

[M2]

$$\min \sum_{v\in V}\{\alpha[L_{1v}q_{1v} + L_{2v}q_{2v}] + \beta_v p_v\} \tag{2.9a}$$

subject to

Constraints (2.4a), (2.6a-e) and

$$q_{1v} \geq \theta_{1vk}\lambda_v + \gamma_{1vk}, q_{1v} \geq 0, \forall k = 1,2,\cdots,K_{1v}, \forall v \in V \tag{2.9b}$$

$$q_{2v} \geq \theta_{2vk}\mu_v + \gamma_{2vk}, q_{2v} \geq 0, \forall k = 1,2,\cdots,K_{2v}, \forall v \in V. \tag{2.9c}$$

Program [M2] can be solved via commercial solvers like CPLEX. However, the computation cost rises rapidly with the number of constraints dictated by K_{1v} and K_{2v} ($v \in V$). To improve the solution efficiency, we develop tighter upper bounds for the optimal λ_v and μ_v than those used in the literature. (For example, in Wang and Meng (2012), the travel time upper bounds were derived from a prespecified minimum speed only.) These better bounds can effectively diminish the search ranges for the optimal λ_v and μ_v, and thus reduce the numbers of linear segments used in constraints (2.8a-b).

Specifically, the following proposition gives the upper bounds of λ_v and μ_v:

Proposition 3. The upper bounds of λ_v and μ_v, denoted by $\lambda_v^{\max}$ and $\mu_v^{\max}$ respectively, are presented as follows:

$$\lambda_v^{\max} = \max\left\{\max\left\{T_v - T_v^0 - \omega - \frac{L_{2v}}{s_v^{\max}}, L_{1v}\left(\frac{\alpha a_v b_v}{\beta_v}\right)^{\frac{1}{b_v+1}}\right\} + 2(|V|-1)H, \frac{L_{1v}}{s_v^{\max}}\right\}, \forall v \in V \tag{2.10a}$$

$$\mu_v^{\max} = \max\left\{T_v - T_v^0 - \omega - \frac{L_{1v}}{s_v^{\max}}, L_{2v}\left(\frac{\alpha a_v b_v}{\beta_v}\right)^{\frac{1}{b_v+1}}, \frac{L_{2v}}{s_v^{\max}}\right\}, \forall v \in V. \tag{2.10b}$$

Proof of Proposition 3 is relegated to Appendix C. In addition, the lower bounds of the optimal λ_v and μ_v are given by (2.6a-b).

Finally, by scrutinizing (2.6c-d), we find that the following value of M is sufficiently large to use:

$$M = H + \max_{v \in V} T_v^0 - \min_{v \in V} T_v^0 + \max_{v \in V} \lambda_v^{\max} - \min_{v \in V} \lambda_v^{\min}. \quad (2.11)$$

Any value greater than (2.11) can also be used. However, using a larger M would increase the solution time of [M2].

2.1.4. A Discrete-time Model

We now discretize the time variables in [M1] using a unit time interval denoted by Δt. Time discretization essentially discretizes the range of speeds each vessel can take in its two sailing legs. Thus, the bunker consumption rate for each discrete speed value can be calculated in advance, eliminating the nonlinearity issue. Note that the travel time bounds developed in Section 2.1.3 also allow us to use as few time intervals as possible, thus improving the computational efficiency of the discrete-time model.

Specifically, define $\tau \in Z_+$ as the integer time coordinate, where Z_+ represents the set of all positive integers. Denote Ψ_{1v} the set of possible arrival times of autonomous vessel $v \in V$ at the bottleneck, and Ψ_{2v} the set of possible travel times of autonomous vessel v from entering the bottleneck to arriving at the destination port. They are given by:

$$\Psi_{1v} = \{\tau | \tau \in Z_+, \frac{1}{\Delta t}(T_v^0 + \lambda_v^{\min}) \leq \tau \leq \frac{1}{\Delta t}(T_v^0 + \lambda_v^{\max})\}, \forall v \in V \quad (2.12a)$$

$$\Psi_{2v} = \{\tau | \tau \in Z_+, \frac{1}{\Delta t}(\omega + \mu_v^{\min}) \leq \tau \leq \frac{1}{\Delta t}(\omega + \mu_v^{\max})\}, \forall v \in V \quad (2.12b)$$

where $\lambda_v^{\min}$, $\lambda_v^{\max}$, $\mu_v^{\min}$, and $\mu_v^{\max}$ are again from Equations (2.6a-b) and Proposition 3 (i.e., Equations (2.10a-b)).

Define two batches of binary decision variables, $x_{\tau v}$ and $\xi_{\tau v}$, to substitute for x_v and y_v. Specifically, $x_{\tau v} = 1$ if and only if $x_v = \Delta t \cdot \tau$, and $\xi_{\tau v} = 1$ if and only if $y_v - x_v = \Delta t \cdot \tau$. We have the following constraints for the discrete-time model:

$$\sum_{\tau \in \Psi_{1v}} x_{\tau v} = 1, \forall v \in V \tag{2.13a}$$

$$\sum_{\tau \in \Psi_{2v}} \xi_{\tau v} = 1, \forall v \in V \tag{2.13b}$$

$$x_{\tau v} \in \{0, 1\}, \forall \tau \in \Psi_{1v}, \forall v \in V \tag{2.13c}$$

$$\xi_{\tau v} \in \{0, 1\}, \forall \tau \in \Psi_{2v}, \forall v \in V. \tag{2.13d}$$

Constraints (2.13a) and (2.13b) will be used to replace (2.2b) and (2.2c) in the original program [M1].

Further denote $\tau_1^{\min} = \min\{\tau \in \cup_{v \in V} \Psi_{1v}\}$ and $\tau_1^{\max} = \max\{\tau \in \cup_{v \in V} \Psi_{1v}\}$ the minimum and maximum arrival times of all autonomous vessels at the bottleneck, and $h' = H/\Delta t$. We select the Δt such that h' is an integer. Then constraints (2.2d) in [M1] can be replaced with the following one, which stipulates that at most one autonomous vessel will arrive at the bottleneck during any h' consecutive time intervals:

$$\sum_{v \in V} \sum_{\tau \in \Psi_{1v} \cap \{i, \ldots, i+h'-1\}} x_{\tau v} \leq 1, \;\; i = \tau_1^{\min}, \tau_1^{\min} + 1, \cdots, \tau_1^{\max} - h' + 1. \tag{2.14}$$

In the discrete-time model, the penalty term in the objective (2.2a), $\beta_v \cdot \max\{0, y_v - T_v\}$, is also linearized as described in Section 2.1.3. The associated constraints (2.4a) are retained, while constraints (2.4b) are replaced with:

$$p_v \geq \sum_{\tau \in \Psi_{1v}} \Delta t \cdot \tau \cdot x_{\tau v} + \sum_{\tau \in \Psi_{2v}} \Delta t \cdot \tau \cdot \xi_{\tau v} - T_v, \forall v \in V. \tag{2.15}$$

This is because $y_v = \sum_{\tau \in \Psi_{1v}} \Delta t \cdot \tau \cdot x_{\tau v} + \sum_{\tau \in \Psi_{2v}} \Delta t \cdot \tau \cdot \xi_{\tau v}$, and $x_v = \sum_{\tau \in \Psi_{1v}} \Delta t \cdot \tau \cdot x_{\tau v}, \forall v \in V$.

Finally, the bunker fuel cost term in (2.2a), $\alpha \left[L_{1v} a_v \left(\frac{L_{1v}}{x_v - T_v^0} \right)^{b_v} + L_{2v} a_v \left(\frac{L_{2v}}{y_v - x_v - \omega} \right)^{b_v} \right]$, is rewritten as $\alpha [L_{1v} Q_{1v} + L_{2v} Q_{2v}]$, where Q_{1v} and Q_{2v} are expressed as functions of $x_{\tau v}$ and $\xi_{\tau v}$:

$$Q_{1v} = a_v \left(\frac{L_{1v}}{\sum_{\tau \in \Psi_{1v}} \Delta t \cdot \tau \cdot x_{\tau v} - T_v^0} \right)^{b_v}, \forall v \in V \quad (2.16a)$$

$$Q_{2v} = a_v \left(\frac{L_{2v}}{\sum_{\tau \in \Psi_{2v}} \Delta t \cdot \tau \cdot \xi_{\tau v} - \omega} \right)^{b_v}, \forall v \in V. \quad (2.16b)$$

Since $x_{\tau v}$ and $\xi_{\tau v}$ are binary variables, (2.16a-b) are equivalent to:

$$Q_{1v} = \sum_{\tau \in \Psi_{1v}} a_v \left(\frac{L_{1v}}{\Delta t \cdot \tau - T_v^0} \right)^{b_v} x_{\tau v}, \forall v \in V \quad (2.17a)$$

$$Q_{2v} = \sum_{\tau \in \Psi_{2v}} a_v \left(\frac{L_{2v}}{\Delta t \cdot \tau - \omega} \right)^{b_v} \xi_{\tau v}, \forall v \in V. \quad (2.17b)$$

In summary, program [M1] can be converted to the following binary integer program:

[M3]

$$\min \sum_{v \in V} \left\{ \alpha \left[L_{1v} \sum_{\tau \in \Psi_{1v}} a_v \left(\frac{L_{1v}}{\Delta t \cdot \tau - T_v^0} \right)^{b_v} x_{\tau v} + L_{2v} \sum_{\tau \in \Psi_{2v}} a_v \left(\frac{L_{2v}}{\Delta t \cdot \tau - \omega} \right)^{b_v} \xi_{\tau v} \right] + \beta_v p_v \right\} \quad (2.18)$$

subject to

Constraints (2.4a), (2.13a-d), (2.14) and (2.15).

[M3] can also be solved by CPLEX.

2.2. Solution Quality and Computational Efficiency

This section looks into the solution quality and computational efficiency of models [M2] and [M3]. We first consider 100 numerical instances with 12 autonomous vessels. The parameters of each instance, i.e., L_{1v}, L_{2v}, T_v^0, T_v, β_v, $s_v^{\max}$, a_v and b_v for $v \in \{1,2,\dots,12\}$, are randomly generated from the following distributions: $L_{1v}, L_{2v} \sim U[31, 360]$ n miles, $T_v^0 \sim U[0.1, 30]$ h, $T_v \sim U[30, 60]$ h, $\beta_v \sim U[1000, 6000]$ \$/h, $s_v^{\max} \sim U[18, 23]$ knot, $a_v \sim U[4, 5] \times 10^{-4}$, $b_v \sim U[1.8, 2.2]$, where $U[c_1, c_2]$ denotes a uniform distribution with support from c_1 to c_2. The distributions of $s_v^{\max}$, a_v and b_v are assumed to follow the values suggested by Wang and Meng (2012). The bunker fuel price α, the autonomous vessel transit time through the bottleneck ω, and the minimum headway H are set to 500 \$/ton, 3.0 h, and 1.0 h, respectively (Sina News, 2020). In addition, we specify seven values of the error bound ε in [M2], i.e., $\varepsilon \in \{625$, 312.5, 156.3, 78.1, 39.1, 19.5, 9.8\} \$, and seven values of the time interval Δt in [M3]: $\Delta t \in \left\{1, \frac{1}{2}, \frac{1}{4}, \frac{1}{8}, \frac{1}{16}, \frac{1}{32}, \frac{1}{64}\right\}$ h. Note that both ε and Δt decrease at a rate of 0.5 in the above sequences. Models [M2] and [M3] are solved by CPLEX-12.8 running on a 4.7 GHz Octa-Core PC with 32 GB of RAM.

Solutions obtained from the two approximate models [M2] and [M3] are plugged into (2.2a) to calculate the true objective values. Thus, the results are upper bounds of the optimal solution. For simplicity, we calculate the averages of each model's objective values and runtimes across the 100 numerical instances. The average values of [M2]

are plotted against ε in Fig. 2.1a, and those of [M3] are plotted against Δt in Fig. 2.1b. Note that the horizontal axis is set to the logarithmic scale in each figure.

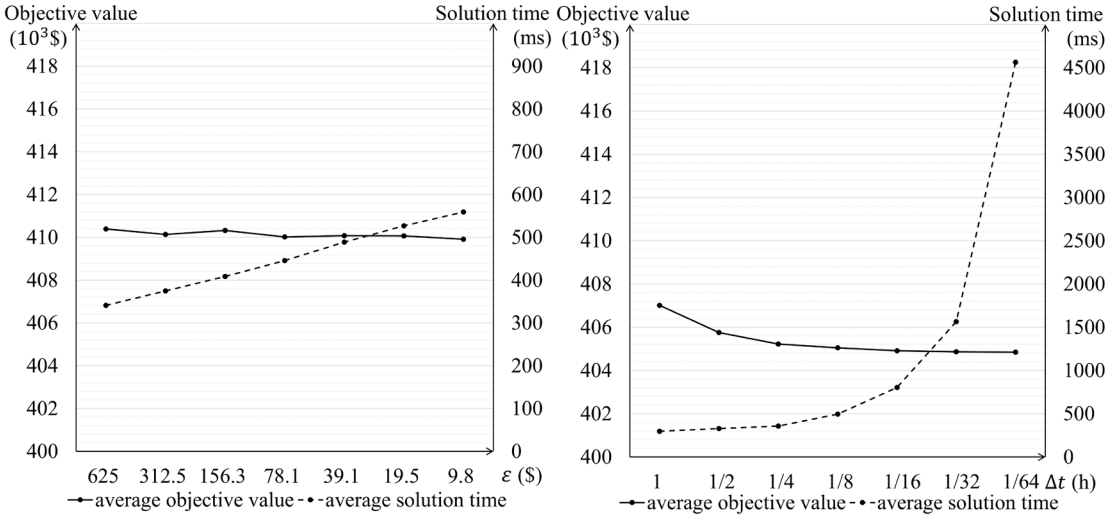

(a) Outer-approximation model [M2] (b) Discrete-time model [M3]

Fig. 2.1. Objective values and solution times of the two models.

Both figures show that the average objective value (the solid curve) decreases as ε and Δt diminish. However, the two solid curves exhibit different patterns. The average objective value calculated from [M3] quickly converges to 4.05×10^5 \$ as $\Delta t \leq \frac{1}{8}$ h, manifesting that the solution to [M3] approaches the exact solution of [M1] as Δt approaches zero. On the other hand, the objective value obtained from [M2] oscillates around 4.10×10^5 when $\varepsilon \leq 312.5$ \$. This reveals that the solution of [M2] has a larger error than that of [M3]. (Recall that the curves show the true objective values calculated by the original objective function (2.2a), and they are upper bounds of the exact solution of [M1].) Using the convergent objective value of [M3] as the benchmark, the solution to [M2] exhibits an error of at least 1.2%. More importantly, further numerical analyses showed that this error did not diminish when ε approaches

zero, meaning the predefined "error bound" ε cannot be guaranteed. These observations are at odds with the theory of the outer-approximation method. We believe the main reason possibly lies in the piecewise linear approximation of nonlinear functions $Q_{1v}(\lambda_v)$ and $Q_{2v}(\mu_v)$. Specifically, numerical error arises when calculating the lines and points of tangency in the piecewise linear approximation of [M2] (see Algorithm 1 in Appendix B). Regrettably, this error tends to fluctuate as ε approaches zero since the start point of each tangent line segment becomes closer to the original curve. Please refer to the end of Appendix B for a more detailed explanation.

On the other hand, the average runtime increases as ε and Δt diminish; see the dashed curves in Fig. 2.1a and b. This observation is expected. The runtime in Fig. 2.1b increases rapidly since the number of constraints in [M3] grows linearly with the number of time intervals; see Equation (2.14). Nevertheless, Fig. 2.1b shows that the solution quality is good enough for $\Delta t \leq \frac{1}{8}$ hour. The benefit of further reducing Δt is negligible.

A more important question is how the two models perform when solving larger-scale instances. Fig. 2.2 plots the average runtimes of 100 randomly selected instances for [M2] and [M3] when the number of vessels $|V|$ varies from 10 to 120. For each value of $|V|$, the same 100 instances are solved by both models. The ε and Δt are set to 1,000 $ and 0.1 h, respectively. These values are selected to favor [M2] in terms of the runtime; see Fig. 2.1a and b. Other values of ε and Δt yield similar results as in Fig. 2.2. The other parameter values are the same as for Fig. 2.1a and b. Fig. 2.2 shows that

the runtime of [M2] soars when $|V| > 20$, making [M2] unacceptably slow for large-scale autonomous vessel scheduling problems. The reason is simple. Note that the number of piecewise linear constraints (2.9b) and (2.9c) in [M2] increases rapidly with $|V|$. Furthermore, the number of constraints (2.6c) and (2.6d) increases quadratically with $|V|$. These problems do not exist for [M3].

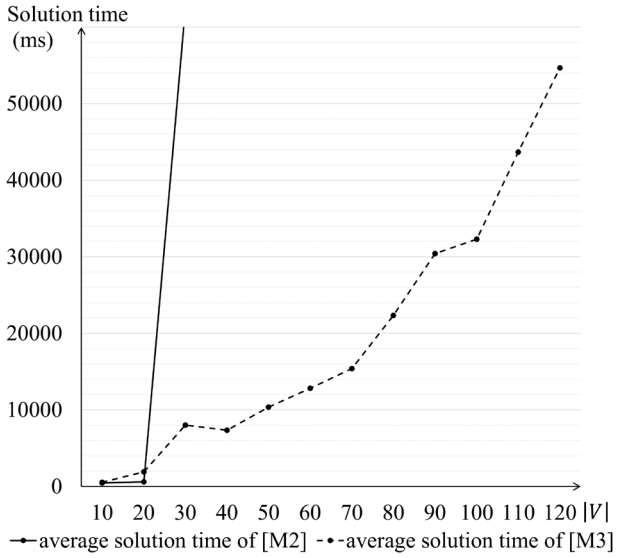

Fig. 2.2. Comparison of solution times of [M2] and [M3] for $|V| \in [10, 120]$.

In summary, [M3] appears to be a better choice than [M2] in terms of both solution quality and computational efficiency, especially for large-scale problems.

2.3. Numerical Study

The background and parameter values of a real-life case study are introduced in Section 2.3.1. Section 2.3.2 examines the optimal autonomous vessel schedules and the associated delays obtained from the two models. The benefit of the optimal

coordination of autonomous vessel passages at the bottleneck is investigated in Section 2.3.3.

2.3.1. Description of the Case Study and Parameter Values

The Three Gorges Dam on the Yangtze River is one of the busiest waterway bottlenecks in the world (Pomfret, 2019). We consider a simple case with 12 autonomous vessels passing through the TGD lock. These autonomous vessels can be remotely controlled and optimally coordinated by a central planner. The maximum sailing speeds and bunker consumption parameters of the 12 autonomous vessels are again borrowed from Wang and Meng (2012) and summarized in Table 2.1. Columns 2–5 of Table 2.2 show the 12 autonomous vessels' origin and destination ports and their distances from the TGD. Locations of these ports and the TGD on the Yangtze River are illustrated in Fig. 2.3. Columns 6–11 of Table 2.2 show their departure and expected arrival times and penalty rates for two scenarios. These parameter values are selected in a way that the autonomous vessels' sailing time windows ($T_v - T_v^0$) in Scenario 1 are generally tighter than in Scenario 2, while the penalty rates in Scenario 2 are higher. By comparing these two scenarios, we can examine how the autonomous vessels' travel time windows and penalty rates β_v affect the optimal autonomous vessel schedules and actual arrival times at the destination ports. The autonomous vessel transit time ω and the minimum headway H are set to 3.0 h and 1.0 h, respectively. Three bunker fuel prices, 200, 500, and 800 \$/ton, are employed to reflect the price fluctuations in the fuel market (Ship and Bunker, 2021). Comparing the solutions under different fuel prices

can unveil how the fuel price affects the optimal autonomous vessel schedules and delays. For the outer-approximation model [M2] (i.e., the continuous-time model), the error bound ε is set to 1,000 \$. For the discrete-time model [M3], the unit time interval Δt is set to 0.1 h.

Table 2.1. Maximum sailing speeds and bunker consumption parameters.

Vessel	1	2	3	4	5	6	7	8	9	10	11	12
$s_v^{\max}$ (knot)	19	20	19	18	21	23	19	18	22	20	21	19
a_v ($\times 10^{-4}$)	4.2	4.0	4.3	4.2	4.3	4.4	4.5	4.1	4.2	4.3	4.1	4.3
b_v	1.95	2.10	1.98	2.05	2.02	1.96	1.89	1.96	2.04	1.97	2.10	2.11

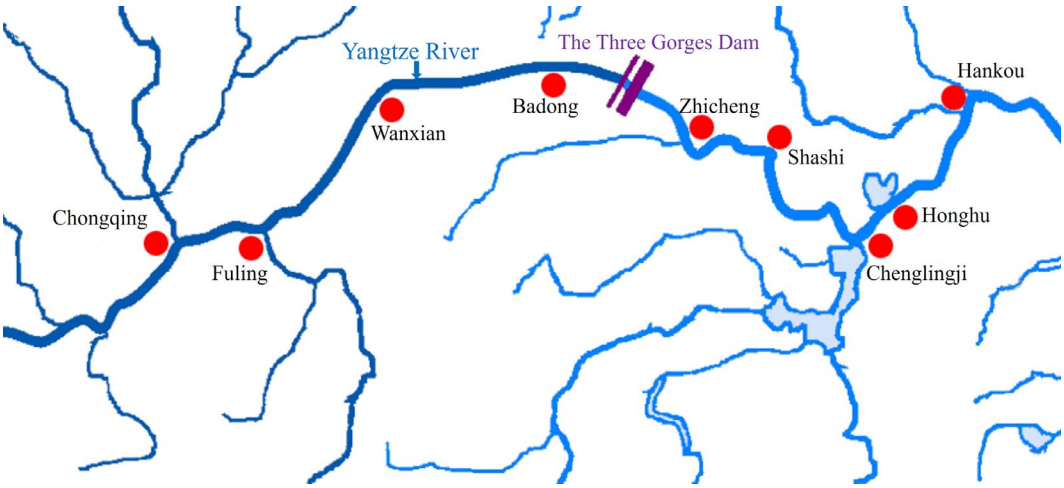

Fig. 2.3. Locations of the origin and destination ports and the TGD along the Yangtze River.

2.3.2. Optimal Autonomous Vessel Scheduling Solutions

Fig. 2.4a and b plot the optimal total cost, the tardiness penalty, and the bunker cost against the bunker price α for the two scenarios, respectively. Results of [M2] and [M3] are plotted as the solid and dashed curves, respectively. Note that the optimal cost values calculated by the two models are very close to each other in most cases. An exception occurs when $\alpha = 800$ \$/ton under Scenario 1, where the gaps in the bunker

cost and the tardiness penalty are 7% and 46%, respectively. These large gaps are possibly due to the inaccuracy of the linear approximation in [M2].

Table 2.2. Vessel route parameters, departure and expected arrival times, and penalty rates.

Vessel	Origin	Destination	L_{1v} (n mile)	L_{2v} (n mile)	Scenario 1			Scenario 2		
					T_v^0 (h)	T_v (h)	β_v ($/h)	T_v^0 (h)	T_v (h)	β_v ($/h)
1	Zhicheng	Badong	51.84	31.86	23.8	32.5	1000	23.3	30.2	4000
2	Zhicheng	Wanxian	51.84	145.79	23.3	41.2	1200	19.7	30.2	4200
3	Shashi	Fuling	101.51	257.56	19.7	47.8	1500	19.7	41.6	4500
4	Shashi	Chongqing	101.51	322.35	23.7	49.8	1900	23.3	41.6	4900
5	Shashi	Badong	101.51	31.86	21.7	31.5	2100	8.2	52.8	4100
6	Chenglingji	Wanxian	234.88	145.79	11.2	40.2	2400	1.3	59.2	4400
7	Chenglingji	Fuling	234.88	257.56	12.5	41.1	3900	1.3	41.6	4900
8	Chenglingji	Chongqing	234.88	322.35	13.5	46.1	5000	10.2	51.2	5000
9	Honghu	Badong	262.96	31.86	10.6	24.7	5200	10.2	59.2	5200
10	Honghu	Wanxian	262.96	145.79	10.1	31.2	5400	8.2	59.2	5400
11	Hankou	Fuling	359.61	257.56	2.3	40.8	5700	1.3	52.8	5700
12	Hankou	Wanxian	359.61	145.79	3.3	36.2	5000	1.3	59.2	5000

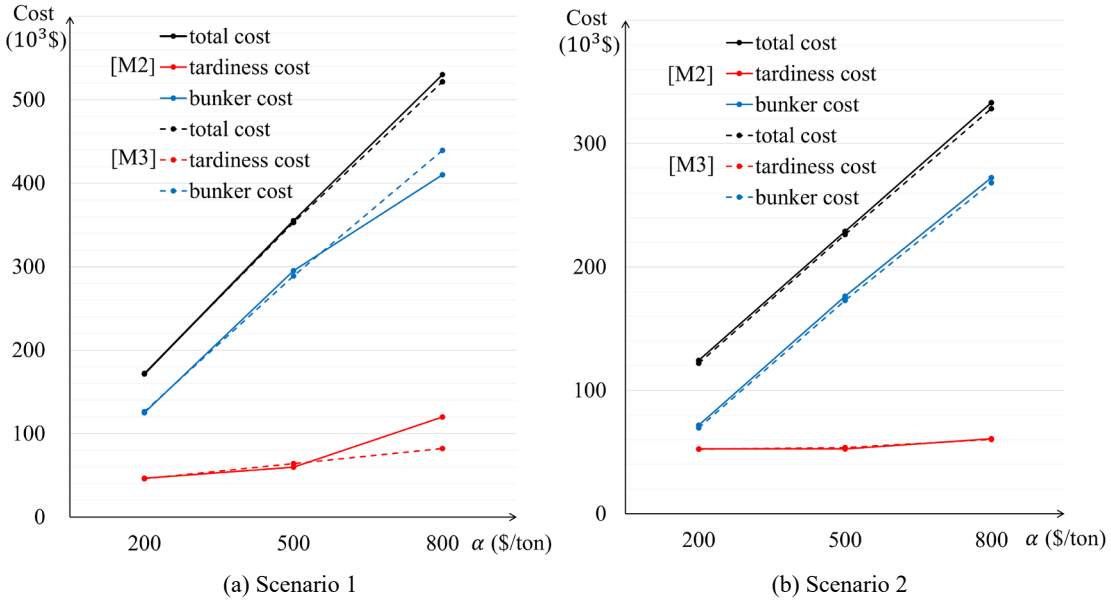

Fig. 2.4. Total cost and cost components versus α.

As expected, the total cost increases rapidly as α grows in each scenario. The increase is mainly due to the surge in the bunker cost. The tardiness penalty also increases since vessels will reduce their speeds to save the bunker at a higher price,

although that would result in larger schedule delays. The difference between the two scenarios is also evident. In Scenario 1, the tardiness penalty increases by 78% (using the more accurate result of [M3]) when α rises from 200 to 800 \$/ton since more vessels choose to bear greater delays with the lower tardiness penalty rates. However, for the same case in Scenario 2, the tardiness penalty only increases by 13% due to the higher penalty rates.

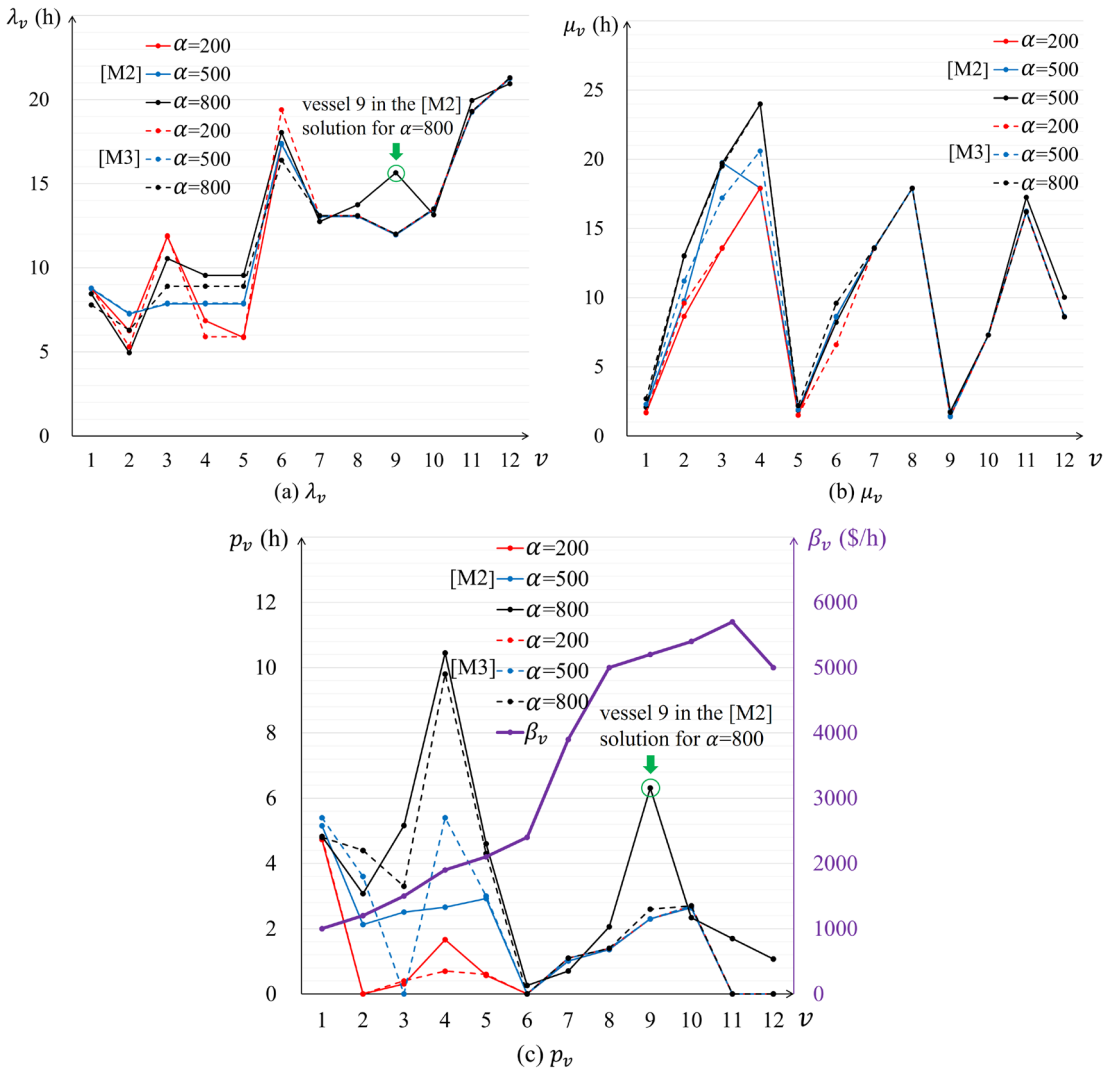

Fig. 2.5. Optimal vessel sailing times and delays under Scenario 1.

We further examine the detailed solutions, i.e., the optimal λ_v, μ_v, and p_v, of [M2] and [M3]. For simplicity, only the results for Scenario 1 are plotted in Fig. 2.5a-c. Similar findings were also observed for Scenario 2 but are omitted here for simplicity. Note that the figures unveil a variety of mismatches between the solid curves (solutions from [M2]) and the dashed ones (solutions from [M3]), especially for autonomous vessel 9 when $\alpha = 800$ \$/ton (see the circled points in Fig. 2.5a and c). It turns out that the two approximate models produced considerably different solutions despite the small ε and Δt used and the similar objective values.

Fig. 2.5a-c also show that the sailing times and delays of autonomous vessels 1-6 at their destinations are moderately sensitive to α. Specifically, the delays roughly increase with α; see Fig. 2.5c. On the other hand, the sailing times and delays of autonomous vessels 7-12 are insensitive to α, possibly because those autonomous vessels have larger penalty rates (see the bold purple curve in Fig. 2.5c). For the same reason, the delays of autonomous vessels 7-12 are relatively low[3].

2.3.3. Benefit of the Optimal Coordination of Vehicle Passages through the Bottleneck

To better understand the benefit of optimal autonomous vessel scheduling, we compare the cost of optimal scheduling against two simpler scheduling strategies.

[3] The delay of autonomous vessel 9 in the [M2] solution for $\alpha = 800$ \$/ton is an exception. This is possibly due to the inaccuracy of the [M2] solution.

The first strategy assumes no central operation manager, meaning that the individual vessels' sailing times are not coordinated. Each vessel optimizes its speed profile without knowing other vessels' arrival times at the bottleneck. When vessels form a queue at the bottleneck, they will pass following the first-come, first-serve (FCFS) rule. Each vessel will then re-optimize its speed for the second sailing leg after passing the bottleneck. The scheduling and cost evaluation model under this FCFS strategy is formulated in Appendix D.

The second strategy assumes that the central operation manager adopts a "naïve" rule to prioritize the vessels with higher penalty rates. Specifically, the manager sorts all the vessels according to their β_v's in descending order. (Thus, we term this strategy the descending-penalty or DP strategy.) The vessel on the top of the list will adopt a speed profile that minimizes its own cost. From the second vessel on, each vessel can pass the bottleneck following its cost-minimizing speed profile if the passage does not conflict with any vessel with a higher β_v. If a conflict occurs, that vessel will have to postpone its passage. After determining all the vessels' passage times at the bottleneck, the central operation manager will re-optimize their speeds to avoid queues. This strategy's scheduling and cost evaluation model is relegated to Appendix E.

We compare the total cost, the tardiness penalty, and the bunker cost under the optimal scheduling strategy, the FCFS strategy, and the DP strategy for the two scenarios of the TGD case in Fig. 2.6a and b. Only the solutions of [M3] are used for comparison because we reckon that they are more accurate than the [M2] solutions.

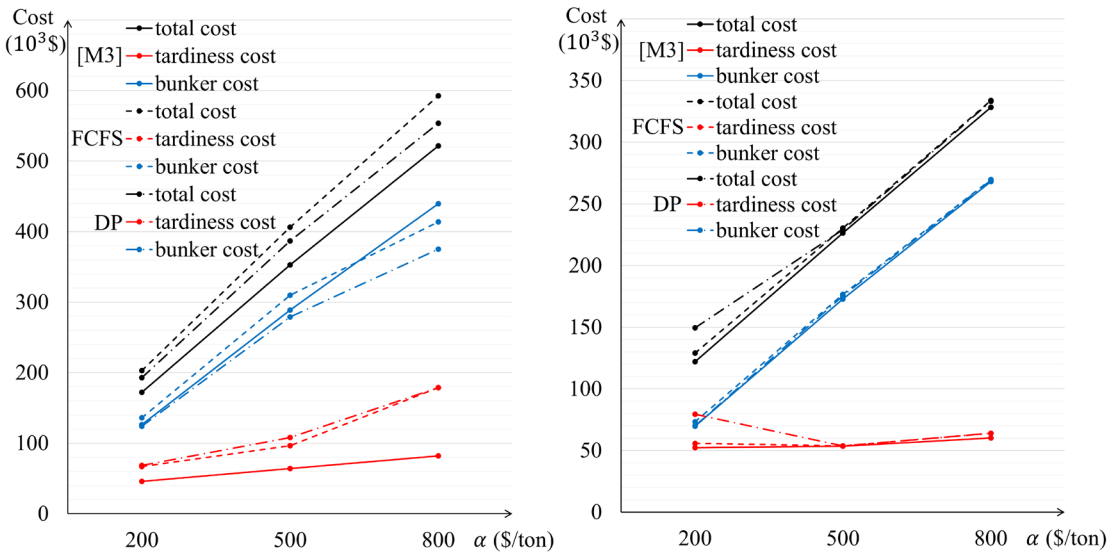

Fig. 2.6. Comparison of the three scheduling strategies.

Fig. 2.6a shows that the optimal scheduling strategy can save up to 12% of the total cost compared to the FCFS strategy with no coordination and 5.8% compared to the DP strategy with naïve coordination. This manifests the considerable cost advantage of the system-optimal coordination and scheduling. Further comparison of the cost components reveals that the tardiness penalty under the optimal strategy is much lower than the two benchmark strategies, which is the main reason for the cost advantage of optimal coordination.

To our surprise, the DP strategy exhibits the highest delay penalty but the lowest bunker cost. This finding is counterintuitive since this strategy aims to reduce the schedule delays of vessels with higher penalty rates. The reason is that some vessels with lower penalty rates have to postpone their passages excessively to make way for those with higher penalty rates, even if the latter vessels arrive at the bottleneck later. As a result, the DP strategy backfires by causing the highest tardiness penalty, indicating

that simply prioritizing vessels according to their penalty rates is ineffective. The lowest bunker cost of this strategy is due to the same reason. After the speed re-optimization, some vessels sail at very slow speeds in the first leg since they have to make way for other vessels at the bottleneck anyway.

On the other hand, Fig. 2.6b shows that the three strategies produce similar costs in Scenario 2 (only the cost under the DP strategy for $\alpha = 200$ \$/ton is moderately higher due to the relatively larger tardiness penalty and the quite low fuel price). This is because most vessels suffer only small penalties due to their wide sailing time windows in Scenario 2, regardless of the strategy. Thus, the room for improvement by optimally coordinating vessel travel is meager.

2.4. Summary

This chapter developed a new nonlinear model for minimizing the sum of autonomous vessels' bunker cost and lateness penalty by selecting the optimal autonomous vessel schedules for passing a common bottleneck and the associated speed profiles. Two linear approximations of the model were proposed. One employed a piecewise linear lower bound to approximate the nonlinear bunker consumption function. The other converted the original model to a binary integer program by discretizing the time. Tighter bounds of autonomous vessel travel times were developed to improve the computational efficiency of both methods.

Comparison via extensive numerical experiments showed that, even though the two approximate models yielded similar objective values (see Fig. 2.4a and b), they produced quite different schedules for individual autonomous vessels (see Fig. 2.5a-c). Scrutinization unveiled that the solution from the discrete-time model [M3] was more accurate than that of the outer-approximation model [M2] (see Fig. 2.1a and b). This is likely due to the errors arising in the numerical computation of the tangent lines and points for [M2] (see Appendix B). These errors may increase as the predefined error bound ε diminishes, thus rendering the theoretical error bound invalid. Moreover, [M3] is much faster than [M2] for large-scale instances (see Fig. 2.2). The findings speak to the limitations of the outer-approximation method in real practice.

Numerical results of the TGD case study unveiled how the bunker price, tightness of the sailing time windows, and the penalty rates affect the optimal autonomous vessel schedules and the minimal cost (see Section 2.3.2). By comparing against a no-coordination strategy and a naïve coordination strategy, we showed that the optimal autonomous vessel scheduling could significantly reduce the cost, especially the tardiness penalty when the sailing time windows were tight. However, when the sailing time windows were very loose, the improvement of optimal autonomous vessel scheduling was small.

Chapter 3. Optimal Scheduling of Autonomous Vessel Trains in a Hub-and-Spoke Network

This chapter develops novel models for jointly optimizing the autonomous vessel assignment to the vessel trains, and the sequence of ports of call and the schedule of each vessel train in a hub-and-spoke network. Two mixed-integer programming models are developed, one for the freight distribution problem and the other for the vessel backhaul problem. Solutions to these models capture the optimal tradeoff between the added detour and delay costs of vessel trains and the lower sailing cost of autonomous ships. Numerical case studies are carried out for a real-world short-sea shipping network around the Bohai Bay of China. Results reveal sizeable cost savings of vessel train operations as compared to using conventional ships only. Sensitivity analyses are performed to unveil how the benefit of vessel trains is affected by key operating factors, e.g., the numbers of conventional and autonomous ships, the ratio between their costs, the maximum vessel train length, and the network topology.

The rest of this chapter is organized as follows. Section 3.1 describes the problem definition, model formulations, and their linearization. Numerical results of the Bohai Bay case study are presented in Section 3.2. Section 3.3 summarizes this chapter. The notation used in this chapter is summarized in Appendix F.

3.1. Problem Description and Formulation

Section 3.1.1 presents the problem setup and key assumptions. Section 3.1.2 formulates the problem as a mixed-integer nonlinear program (MINLP). Section 3.1.3 linearizes the original program. The backhaul problem of vessel trains is discussed in Section 3.1.4.

3.1.1. Problem Setup

Consider a regional waterway transportation network represented by a set of ports $P \equiv \{0, 1, \dots, |P|\}$, including a hub port numbered 0, and feeder ports $i \in P\backslash\{0\}$. We first investigate a freight distribution problem where the cargoes are loaded to the vessels (conventional or autonomous) at the hub port and transported to the feeder ports. A backhaul problem, i.e., the freight collection problem where vessels (carrying cargoes or not) travel from the feeder ports to the hub port, will be discussed in Section 3.1.4. Denote $L \equiv \{1, 2, \dots, |L|\}$ the set of conventional manned ships that can serve as leader ships of vessel trains, and $F \equiv \{|L| + 1, \dots, |L| + |F|\}$ the set of autonomous ships. Each vessel train consists of one leader vessel, denoted by $l \in L$, and n_l autonomous follower ships. We specify that $0 \leq n_l \leq u_l$ where u_l denotes the maximum number of follower ships led by l. The leader vessel sails solo if $n_l = 0$. With a slight abuse of notation, we also use l to indicate that vessel train led by l.

The destination port of leader vessel $l \in L$ is denoted by d_l and that of autonomous follower vessel $f \in F$ is denoted by d_f, $d_l, d_f \in P\backslash\{0\}$. Vessel train l may

call several ports to drop off the follower ships before arriving at the leader's destination d_l. Denote T_l and T_f the earliest departure times of $l \in L$ and $f \in F$ from the hub port, and T_l' and T_f' their expected arrival times at the destination ports, respectively. A penalty will be imposed on a ship that arrives later than the expected arrival time. This penalty will be calculated by the delay multiplied by a predefined penalty cost rate. The penalty cost rate is denoted by p_l for $l \in L$ and p_f for $f \in F$. We assume that the sailing time from port $i \in P$ to port $j \in P$, denoted by $t_{i,j}$, is identical for all the vessels and vessel trains. Further assume that the sailing cost, including the fuel, operating, crew, and vessel renting costs, is proportional to the travel time. Denote c_l and c_f the sailing cost per unit travel time for $l \in L$ and $f \in F$, respectively.

The objective is to minimize the sum of the sailing cost and the penalty for all the vessels. The optimal decision is concerned with: (i) how the autonomous vessels are assigned to the leader vessels to form vessel trains; and (ii) when each vessel train departs from the hub port and in what order it calls each member ship's destination port.

3.1.2. Mathematical Formulation

[P0]

$$\min \sum_{l\in L}[c_l\lambda_l + p_l(\tau_l + \lambda_l - T_l')^+] + \sum_{f\in F}\left[c_f\lambda_f + p_f\left(\tau_f + \lambda_f - T_f'\right)^+\right] \tag{3.1}$$

subject to

$$\sum_{l\in L}\phi_{l,f} = 1,\ \forall f \in F \tag{3.2}$$

$$\sum_{f\in F}\phi_{l,f} \le u_l,\ \forall l \in L \tag{3.3}$$

$$\tau_f \ge T_f,\ \forall f \in F \tag{3.4}$$

$$\tau_f \geq \tau_l - M\left(1 - \phi_{l,f}\right),\ \forall l \in L, \forall f \in F \tag{3.5}$$

$$\tau_l \geq T_l,\ \forall l \in L \tag{3.6}$$

$$\tau_l \geq \phi_{l,f} T_f,\ \forall l \in L,\ \forall f \in F \tag{3.7}$$

$$\lambda_f \geq t_{0,d_f},\ \forall f \in F \tag{3.8}$$

$$\lambda_f \geq \lambda_k + t_{d_k,d_f} - M\left(1 - \beta_{k,f}^l\right),\ \forall l \in L,\ \forall f,k \in F, f \neq k \tag{3.9}$$

$$\sum_{k\in F} \sum_{f\in F, f\neq k} \beta_{k,f}^l \geq \sum_{f\in F} \phi_{l,f} - 1,\ \forall l \in L \tag{3.10}$$

$$\sum_{f\in F, f\neq k} \beta_{k,f}^l \leq 1,\ \forall l \in L, \forall k \in F \tag{3.11}$$

$$\lambda_l \geq t_{0,d_l},\ \forall l \in L \tag{3.12}$$

$$\lambda_l \geq \lambda_f + t_{d_f,d_l} - M\left(1 - \phi_{l,f}\right),\ \forall l \in L,\ \forall f \in F \tag{3.13}$$

$$\tau_f \geq 0,\ \forall f \in F \tag{3.14}$$

$$\tau_l \geq 0,\ \forall l \in L \tag{3.15}$$

$$\lambda_f \geq 0,\ \forall f \in F \tag{3.16}$$

$$\lambda_l \geq 0,\ \forall l \in L \tag{3.17}$$

$$\phi_{l,f} \in \{0,1\},\ \forall l \in L,\ \forall f \in F \tag{3.18}$$

$$\beta_{k,f}^l \in \{0,1\},\ \forall l \in L,\ \forall f,k \in F, f \neq k. \tag{3.19}$$

The two terms of objective (3.1) are the total costs for manned leaders and autonomous followers, respectively, where decision variables τ_l and τ_f denote the actual departure times of leader vessel $l \in L$ and autonomous vessel $f \in F$ from the hub port, respectively; λ_l and λ_f denote the sailing times of vessel l and f from the hub port to their destination ports, respectively; and function $(\quad)^+$ returns the maximum of 0 and the argument.

Constraint (3.2) guarantees that each autonomous vessel is led by one leader vessel, where binary decision variable $\phi_{l,f}$ indicates whether autonomous vessel f is assigned to vessel train l. Constraint (3.3) specifies the capacity of each vessel train. Constraint (3.4) indicates that an autonomous vessel's actual departure time from the hub port is not earlier than that vessel's earliest departure time; and constraint (3.5) stipulates that an autonomous vessel's actual departure time is not earlier than the actual departure time of its leader vessel (i.e., the vessel train), where M is a sufficiently large number whose value will be given momentarily. Constraints (3.6) and (3.7) indicate that a vessel train's actual departure time from the hub port is not earlier than each member vessel's earliest departure time. Constraint (3.8) guarantees that the sailing time of the first autonomous vessel dropped off by vessel train l is not less than the direct sailing time from the hub port to its destination port. Constraint (3.9) ensures that any successive autonomous vessel f's sailing time is not less than the sailing time of its preceding ship in the same vessel train plus the direct sailing time between the two ships' destination ports. The binary decision variable $\beta_{k,f}^{l}$ denotes whether vessel f is successive to vessel k in vessel train l (i.e., f is dropped off right after k). Constraint (3.10) indicates that the sum of $\beta_{k,f}^{l}$ for a specific vessel train l is not less than the number of follower ships assigned to that vessel train minus 1. Constraint (3.11) ensures that each autonomous vessel k has at most one successive vessel in a vessel train. Constraints (3.12) and (3.13) specify that leader vessel l's sailing time must be greater than or equal to: (i) the direct sailing time from the hub port to its destination; and (ii) the sailing time

of any follower f led by l plus the direct sailing time between the two ships' destination ports. Constraints (3.14)-(3.19) define the bounds of continuous decision variables τ_l, τ_f, λ_l, λ_f, and binary variables $\phi_{l,f}$ and $\beta_{k,f}^{l}$.

By scrutinizing (3.4-3.7), (3.9) and (3.13), we find that the following value of M is sufficiently large to use:

$$M = \max\left\{\max_{l\in L} T_l\,, \max_{f\in F} T_f\,, (|F|+1)\cdot \max_{i,j\in P} t_{i,j}\right\}. \tag{3.20}$$

Any value greater than (3.20) can also be used. However, using a larger M would increase the solution time.

3.1.3. Linearization of [P0]

The nonlinear operator $(\cdot)^+$ in objective (3.1) can be simply linearized by introducing auxiliary variables θ_l and θ_f denoting the tardiness of ship $l \in L$ and $f \in F$, respectively. The linearized program is presented as follows:

[P1]

$$\min \textstyle\sum_{l\in L}[c_l\lambda_l + p_l\theta_l] + \sum_{f\in F}\left[c_f\lambda_f + p_f\theta_f\right] \tag{3.21}$$

subject to

Constraints (3.2)-(3.19)

$$\theta_l \geq \tau_l + \lambda_l - T_l',\ \forall l \in L \tag{3.22}$$

$$\theta_f \geq \tau_f + \lambda_f - T_f',\ \forall f \in F \tag{3.23}$$

$$\theta_l \geq 0,\ \forall l \in L \tag{3.24}$$

$$\theta_f \geq 0, \ \forall f \in F. \tag{3.25}$$

As a standard mixed-integer linear program, [P1] can therefore be easily solved by the commercial solvers (e.g., CPLEX) that take advantage of distributed parallel algorithms for mixed-integer linear programming. However, the computational performance will obviously be affected by the problem size. Specifically, given the binary variables $\phi_{l,f}$ and $\beta_{k,f}^{l}$, the number of leader ships $|L|$ and the number of autonomous ships $|F|$ will have a significant impact on the solution time. In addition, the tightness of vessel sailing time windows will also affect the computational performance. The details of the computational performance will be elaborated in the following numerical study section.

3.1.4. The Backhaul Problem

For long-term vessel train operations, the leader and follower ships distributed to the feeder ports must return to the hub port (with or without cargo) to serve more distribution trips. The autonomous ships still need to form vessel trains led by conventional ships when they return. This backhaul problem is the reverse of the above freight distribution problem.

Similarly, we assume that each backhaul ship is associated with an earliest departure time from its origin feeder port and an expected arrival time at the hub port. The other parameters and variables of the backhaul problem are nearly the same as those defined for the freight distribution problem (see Section 3.1.1). Thus, we use the

same notations listed in Appendix F for the backhaul problem. Only trivial changes need to be noted. For example, d_l and d_f now represent the origin ports of the ships, and $\beta_{k,f}^{l}$ now indicates whether autonomous ship f is picked up by leader vessel l preceding autonomous ship k or not. If a backhaul ship carries no load, its expected arrival time can be set to a large value, and its cost and penalty rates can be set to a low value or zero.

Formulation [P1] can be applied to the backhaul problem with only two changes. First, constraint (3.5) should be replace with $\tau_f + \lambda_f \geq \tau_l + \lambda_l - M\left(1 - \phi_{l,f}\right), \forall l \in L, \forall f \in F$. This indicates that an autonomous ship assigned to vessel train l cannot arrive at the hub port earlier than its leader vessel. Second, constraint (3.7) should be replaced with $\tau_l + \lambda_l \geq T_f + \lambda_f - M\left(1 - \phi_{l,f}\right), \forall l \in L, \forall f \in F$. This ensures that a leader vessel cannot pick up an autonomous ship before the latter's earliest departure time. Thus, the backhaul problem is formulated as:

[P2]

$$\min \sum_{l \in L}[c_l \lambda_l + p_l \theta_l] + \sum_{f \in F}\left[c_f \lambda_f + p_f \theta_f\right] \tag{3.26}$$

subject to

Constraints (3.2)-(3.4), (3.6), (3.8)-(3.19), (3.22-3.25)

$$\tau_f + \lambda_f \geq \tau_l + \lambda_l - M\left(1 - \phi_{l,f}\right), \forall l \in L, \forall f \in F \tag{3.27}$$

$$\tau_l + \lambda_l \geq T_f + \lambda_f - M\left(1 - \phi_{l,f}\right), \forall l \in L, \forall f \in F. \tag{3.28}$$

3.2. Numerical Study

We conduct extensive numerical experiments on the freight distribution problem for a case study of the Bohai Bay of China. The backhaul problem is omitted for brevity since the two problems have similar formulations. All the numerical instances are solved by the CPLEX solver (version 12.8) on a personal computer equipped with an Intel Core eight-core processor clocked at 4.7 gigahertz and 32GB RAM clocked at 3200 megahertz.

The background and parameter values of the case study are introduced in Section 3.2.1. Section 3.2.2 examines the computational performance of [P1]. Sections 3.2.3-3.2.7 present the sensitivity analyses of the vessel train operation's cost saving with respect to: (i) the cost ratio between an autonomous ship and a conventional one; (ii) the penalty cost rate; (iii) the tightness of sailing time windows; (iv) the vessel train size limit u_l; and (v) the waterway transportation network topology.

3.2.1. Description of the Case Study and Parameter Values

We consider the waterway transportation network between nine seaports around the Bohai Bay as shown in Fig. 3.1. The Port of Tianjin is the largest port in Northern China. It is thus designated as the hub port. The rest are assumed to be feeder ports. The travel distances between any two of the nine ports are given in Table 3.1. The vessel sailing speed is set to 15 knots (Colling and Hekkenberg, 2020). The travel times, $t_{i,j}$ $(i, j \in P)$, can be calculated by dividing the sailing distance by the sailing speed.

For simplicity, we assume that all the conventional ships are identical and have the same sailing cost rate, i.e., $c_l = c_{\mathcal{L}} = 500$ \$/h, $\forall l \in L$ (Colling and Hekkenberg, 2020). A similar assumption is made for all the autonomous ships. Since the practical cost data for autonomous ships are unavailable, we assume that an autonomous ship's sailing cost rate, $c_f = c_{\mathcal{F}}$, $\forall f \in F$, is expressed as a ratio $0 < \alpha \leq 1$ times $c_{\mathcal{L}}$; i.e., $c_{\mathcal{F}} = \alpha c_{\mathcal{L}}$. The use of α is convenient for the sensitivity analyses. More advanced autonomous ships would have lower α values. We further assume that the penalty cost rates, p_l and p_f, are equal and expressed as a ratio ρ times the sailing cost rate of a conventional ship; i.e., $p_l = p_f = \rho c_{\mathcal{L}}$ ($\forall l \in L$, $f \in F$). Unless otherwise specified, we set $\alpha = 0.7$ (Colling and Hekkenberg, 2020) and $\rho = 0.4$ (Zhang and Wang, 2020) in the following sections.

Fig. 3.1. Positions of the nine seaports in the hub and spoke network.

Each ship's destination feeder port, d_l ($l \in L$) or d_f ($f \in F$), is selected randomly from the eight feeder ports. Their earliest departure times are randomly generated from a uniform distribution over $[0, 24]$ h, i.e., $T_l, T_f \sim \mathrm{U}[0, 24], \forall l \in L, f \in F$. We further specify that the sailing time window for a vessel is expressed by the minimum sailing time duration (i.e., t_{0,d_l} or t_{0,d_f}) times a slack coefficient denoted by δ_l for $l \in L$ and δ_f for $f \in F$. In other words, we set $T_l' = T_l + \delta_l t_{0,d_l}$ and $T_f' = T_f + \delta_f t_{0,d_f}$, where $\delta_l, \delta_f \geq 1$. A smaller slack coefficient means the corresponding vessel's time window is tighter. If $\delta_l = 1$, then the only way for vessel l to avoid a penalty is to depart the hub port immediately at T_l and take a direct sailing route to its destination. Coefficients δ_l and δ_f are also randomly generated from a uniform distribution: $\delta_l, \delta_f \sim \mathrm{U}[\bar{\delta} - \Delta, \bar{\delta} + \Delta]$, where $\bar{\delta}$ denotes the mean slack coefficient, and Δ indicates how varied the coefficients are. We set $\bar{\delta} = 1.3$ and $\Delta = 0.3$ unless otherwise specified.

Table 3.1. Sailing distances (n mile) between any two ports of the case study.

Port ID	0	1	2	3	4	5	6	7	8
	Tianjin	Dandong	Dalian	Lvshun	Yingkou	Qinhuangdao	Yantai	Qingdao	Lianyungang
0	0	335	220	164	266	134	203	443	511
1	335	0	135	201	338	283	195	332	400
2	220	135	0	86	223	168	90	278	346
3	164	201	86	0	162	107	101	309	377
4	266	338	223	162	0	173	227	446	514
5	134	283	168	107	173	0	172	391	459
6	203	195	90	101	227	172	0	247	315
7	443	332	278	309	446	391	247	0	102
8	511	400	346	377	514	459	315	102	0

Source: Marine Distance Tables for China Coast (NGDCNH, 2009).

We also assume all the vessel trains have the same size limit, i.e., $u_l = u, \forall l \in L$. For now, we specify $u = |F|$, meaning that no limitation on the vessel train size is imposed (note that $|F|$ is the total number of autonomous vessels). This renders the most optimistic case. Other values of u_l will be examined in Section 3.2.6.

3.2.2. Computational Performance

We first examine the computational performance for instances where $|L| \in \{4, 6, 8, 10, 12\}$ and $|F| \in \{8, 16, 24, 32, 40, 48, 56, 64\}$. For each $(|L|, |F|)$, ten numerical instances are solved with randomly generated d_l, d_f, T_l, T_f, δ_l, and δ_f ($l \in L$, $f \in F$) from distributions specified in Section 3.2.1. Denote $\bar{T}_{\text{CPU}}^{|L|,|F|}$ the average CPU time for solving the ten instances with $|L|$ leader vessels and $|F|$ followers.

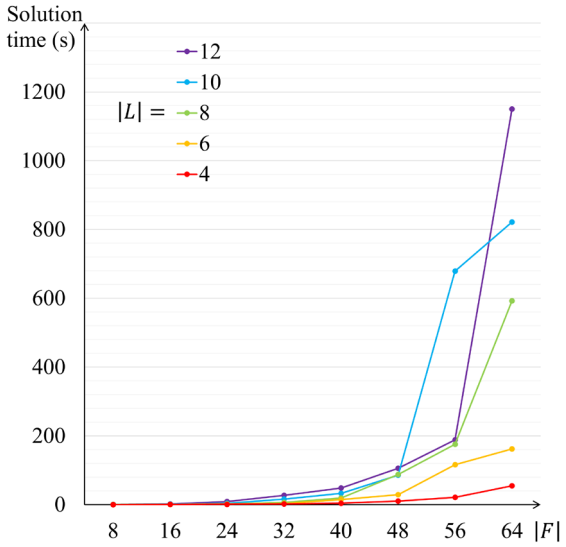

Fig. 3.2. Average solution times of [P1].

Fig. 3.2 plots $\bar{T}_{\text{CPU}}^{|L|,|F|}$ against $|F|$ for different values of $|L|$. The curves show that $\bar{T}_{\text{CPU}}^{|L|,|F|}$ increases rapidly with $|F|$ and $|L|$ with an exception that $\bar{T}_{\text{CPU}}^{|10|,|56|} > \bar{T}_{\text{CPU}}^{|12|,|56|}$. The exception is probably due to the randomness in parameter values. When $|F| \leq 32$,

an instance takes less than 40 seconds to solve on average. However, for a large instance with $|F| = 64$ and $|L| = 12$, the average CPU time is around 20 minutes. Thus, one may need to resort to heuristic methods for even larger-scale instances (which are not common in reality).

The computational efficiency is also significantly affected by the tightness of sailing time windows. This can be seen from Fig. 3.3, which plots the average CPU time of ten randomly generated instances against $\bar{\delta} \in \{1, 1.5, 2, 2.5, 3, 3.5, 4\}$. The case of $\bar{\delta} = 1$ indicates that no slack is available for any vessel. The value of Δ is set to 0 if $\bar{\delta} = 1$ and 0.5 otherwise. We set $|L| = 8$ and $|F| = 24$. All the instances have the same vessel OD pairs and earliest departure times. Only the expected arrival times T_l' and T_f' vary according to $\bar{\delta}$.

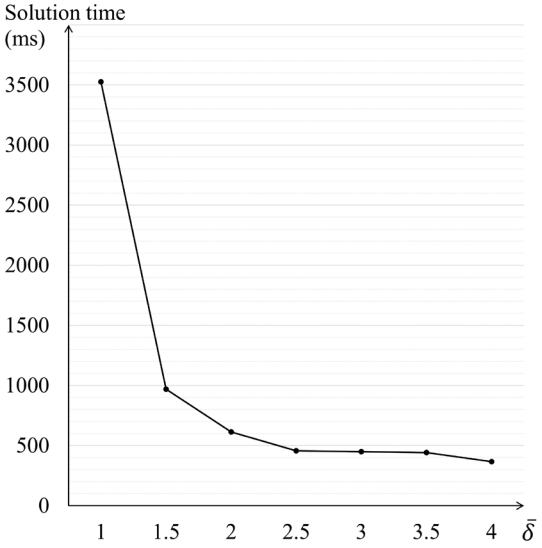

Fig. 3.3. Average solution times against $\bar{\delta}$.

Fig. 3.3 shows that the CPU time plunges as $\bar{\delta}$ grows from 1 to 1.5. This indicates that instances with loose sailing time windows can be solved much faster. When $\bar{\delta}$ continues to grow, the solid cuve decreases slowly and gradually becomes flat.

3.2.3. Sensitivity of the Cost Saving of Vessel Trains to the Cost Rate of Autonomous Vessels

We first examine the sensitivity of the vessel train strategy's cost saving to the ratio between the sailing cost rates of autonomous and conventional ships, i.e., $\alpha = \frac{c_{\mathcal{F}}}{c_{\mathcal{L}}}$. The cost saving is calculated by comparing the overall cost of vessel trains against a benchmark scenario where all the vessels are conventional ones with the same cost and penalty rates. The parameter values are the same between the vessel-train and benchmark scenarios. Note in the latter scenario that each ship will travel individually and directly to its destination.

Specifically, we denote $r^{|L|,|F|}$ the percentage cost saving of the vessel train strategy with $|L|$ conventional leaders and $|F|$ autonomous followers over the benchmark scenario with $|L| + |F|$ conventional, manned vessels; i.e.,

$$r^{|L|,|F|} = (\mathrm{TC}_0^{|L|+|F|} - \mathrm{TC}^{|L|,|F|})/\mathrm{TC}_0^{|L|+|F|}, \tag{3.29}$$

where $\mathrm{TC}^{|L|,|F|}$ and $\mathrm{TC}_0^{|L|+|F|}$ denote the minimum total costs of the vessel train strategy and the benchmark scenario, respectively. We further denote $\xi^{|L|,|F|}$ the share of penalty, $\mathrm{PC}^{|L|,|F|}$, in the overall cost for the vessel train case; i.e.,

$$\xi^{|L|,|F|} = \mathrm{PC}^{|L|,|F|}/\mathrm{TC}^{|L|,|F|}, \tag{3.30}$$

We specify that $|L| = 8$ and $|F| \in \{4, 8, 16, 32\}$. For each $|F|$, ten instances with distinct vessel ODs and time windows are generated randomly. For each instance, we let α vary from 0.5 to 1.0 at an interval of 0.1.[4] Average results of $r^{|L|,|F|}$ and $\xi^{|L|,|F|}$ across the ten test instances are plotted against α in Fig. 3.4a and b, respectively.

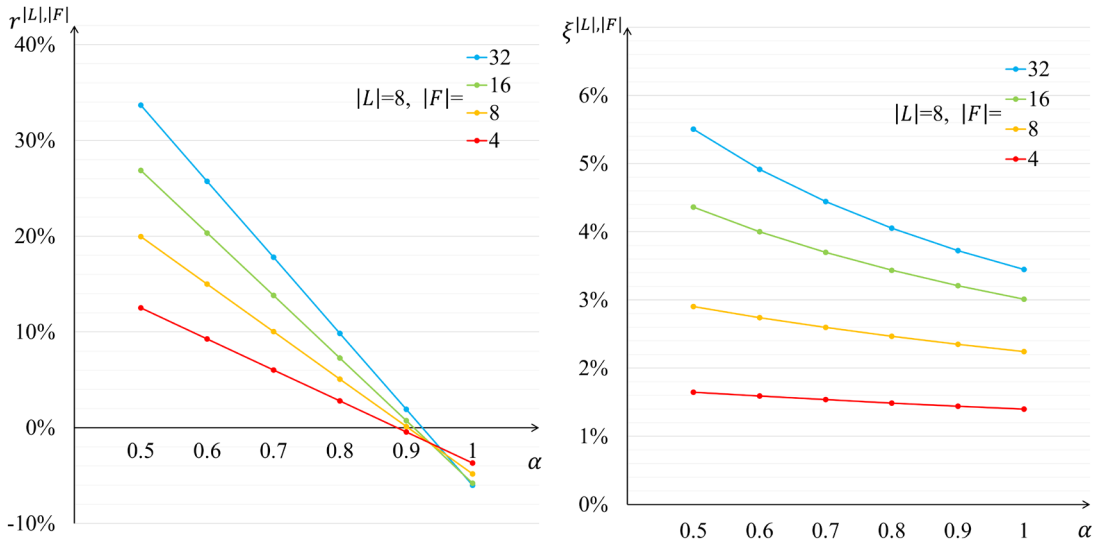

(a) Percentage cost saving

(b) Ratio of penalty to the total cost

Fig. 3.4. Percentage cost saving and share of penalty cost against α for vessel train operations.

As expected, the curves in Fig. 3.4a decrease with α. More importantly, Fig. 3.4a shows that the cost saving increases with the number of autonomous ships (except for the case where $\alpha = 1$), although a larger $|F|$ also means longer vessel trains and thus more detours and delays. For example, when there are 8 leader vessels and 32 autonomous ones, the optimal vessel train assignment plan and schedule can save up to 34% of the cost for $\alpha = 0.5$. Moderate cost savings (3-10%) can be attained even when $\alpha = 0.8$. This speaks to the great potential of autonomous vessel train operations.

[4] The lower bound of α is determined as per Colling and Hekkenberg (2020), where the crew cost is estimated to be 48% of the total.

The curves in Fig. 3.4a are approximately linear because over 90% of the total cost is the sailing cost, which is roughly a linear function of α. This can be seen from Fig. 3.4b. The latter figure shows that the share of penalty cost is less than 6% for all the cases investigated here. The penalty cost takes a larger share when α is small and when there are more autonomous ships (so that the vessel trains are longer and more detours are incurred). This is also as expected.

3.2.4. Sensitivity to the Ratio of Penalty Cost Rate

In this section, we fix the sailing cost rates and let the ratio between the penalty rate and the leader vessels' sailing cost rate, ρ, vary. We set $|L| = 8$ and $|F| \in \{4, 8, 12, 16, 20\}$. Ten randomly generated instances are examined for each $|F|$ and the average $r^{|L|,|F|}$ and $\xi^{|L|,|F|}$ are calculated. We let ρ increase from 0.125 to 8 at a rate of 2. In other words, the penalty rates, $p_{\mathcal{L}}$ and $p_{\mathcal{F}}$, take values in $\{62.5, 125, 250, 500, 1000, 2000, 4000\}$ \$/h. A larger ρ indicates that vessels will try harder to complete their trips by the expected arrival times.

The results of $r^{|L|,|F|}$ and $\xi^{|L|,|F|}$ are plotted in Fig. 3.5a and b, respectively. Fig. 3.5a shows that the cost saving decreases as the penalty rate increases. This is because no penalty is incurred in the benchmark scenario. The cost advantage of vessel train operations is observed for $\rho \leq 2$, meaning that vessel trains (with detours) are unsuitable for the shipment of highly time-sensitive goods. In addition, the sensitivity of cost saving to ρ is higher for larger values of $|F|$, meaning that longer vessel trains

transporting time-insensitive goods can achieve greater cost savings. This is confirmed by Fig. 3.5b. Note that the share of penalty cost is higher for $|F| \geq 12$.

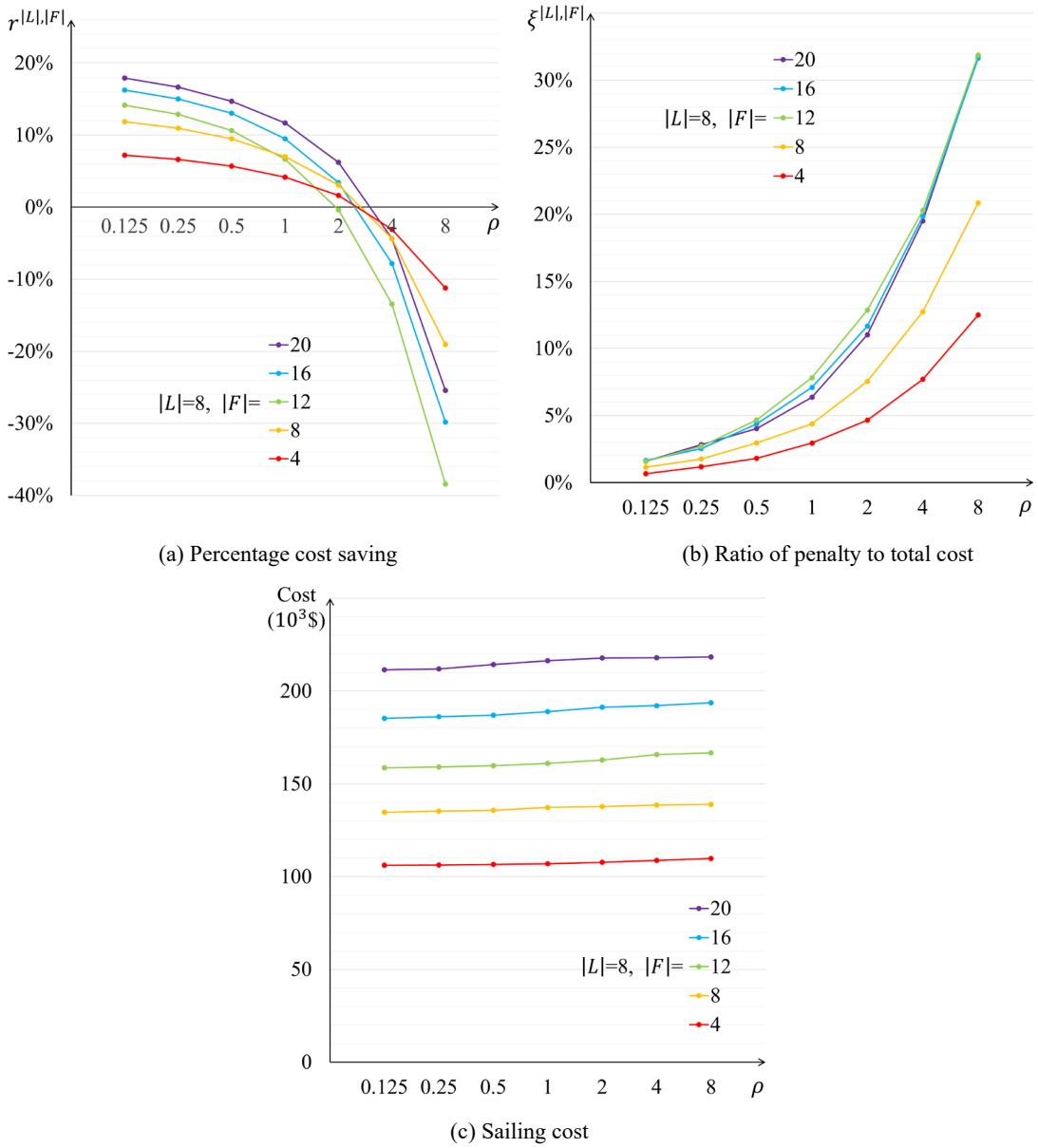

(a) Percentage cost saving

(b) Ratio of penalty to total cost

(c) Sailing cost

Fig. 3.5. Percentage cost saving, share of penalty cost, and sailing cost against ρ.

Fig. 3.5c plots the sailing cost against ρ. The figure shows that the sailing cost is almost insensitive to ρ. In fact, it only increases slightly as ρ grows. This occurs because there is not much room to adjust the optimal vessel assignment and routing when ρ is high. Such stable sailing cost essentially indicates that the vessels'

assignment and routing nearly do not change given that the average number of autonomous vessels led by every leader vessel is basically fixed by the problem formulation.

3.2.5. Sensitivity to the Tightness of Sailing Time Windows

In addition to the cost parameters, one may also be interested in knowing how the cost saving of vessel trains is affected by the tightness of sailing time windows (which also reflects the time sensitivity of the cargo to some degree). Thus, we plot $r^{|L|,|F|}$, $\xi^{|L|,|F|}$ and the sailing cost against $\bar{\delta} \in \{1.0, 1.5, 2.0, 2.5, 3.0, 3.5, 4.0\}$ in Fig. 3.6a-c, respectively. We still set $|L| = 8$ and $|F| \in \{4, 8, 12, 16, 20\}$. The Δ is set to 0 when $\bar{\delta} = 1.0$ and 0.5 otherwise. Each point in Fig. 3.6a-c still represents the average value of ten randomly generated instances.

Fig. 3.6a shows that the cost saving grows with $\bar{\delta}$, which is as expected. The growth rate declines significantly as $\bar{\delta} \geq 2$, revealing that the benefit of vessel train operations is approaching its maximum. This is confirmed by Fig. 3.6b, which manifests that the penalty cost drops drastically below 2% of the total when $\bar{\delta} \geq 2$. When $\bar{\delta} = 4$, the penalty cost is negligible. Comparison across different values of $|F|$ in Fig. 3.6a unveils that the cost saving is slightly more sensitive to $\bar{\delta}$ for a larger $|F|$. This is because longer vessel trains tend to have higher penalty costs. Lastly, Fig. 3.6c shows that the sailing cost is also insensitive to $\bar{\delta}$. According to the problem formulation, the number of leader vessels and the number of autonomous vessels are actually the

most important factors that determine the average vessel assignment and routing which can directly affect the total sailing cost of the whole vessel train system.

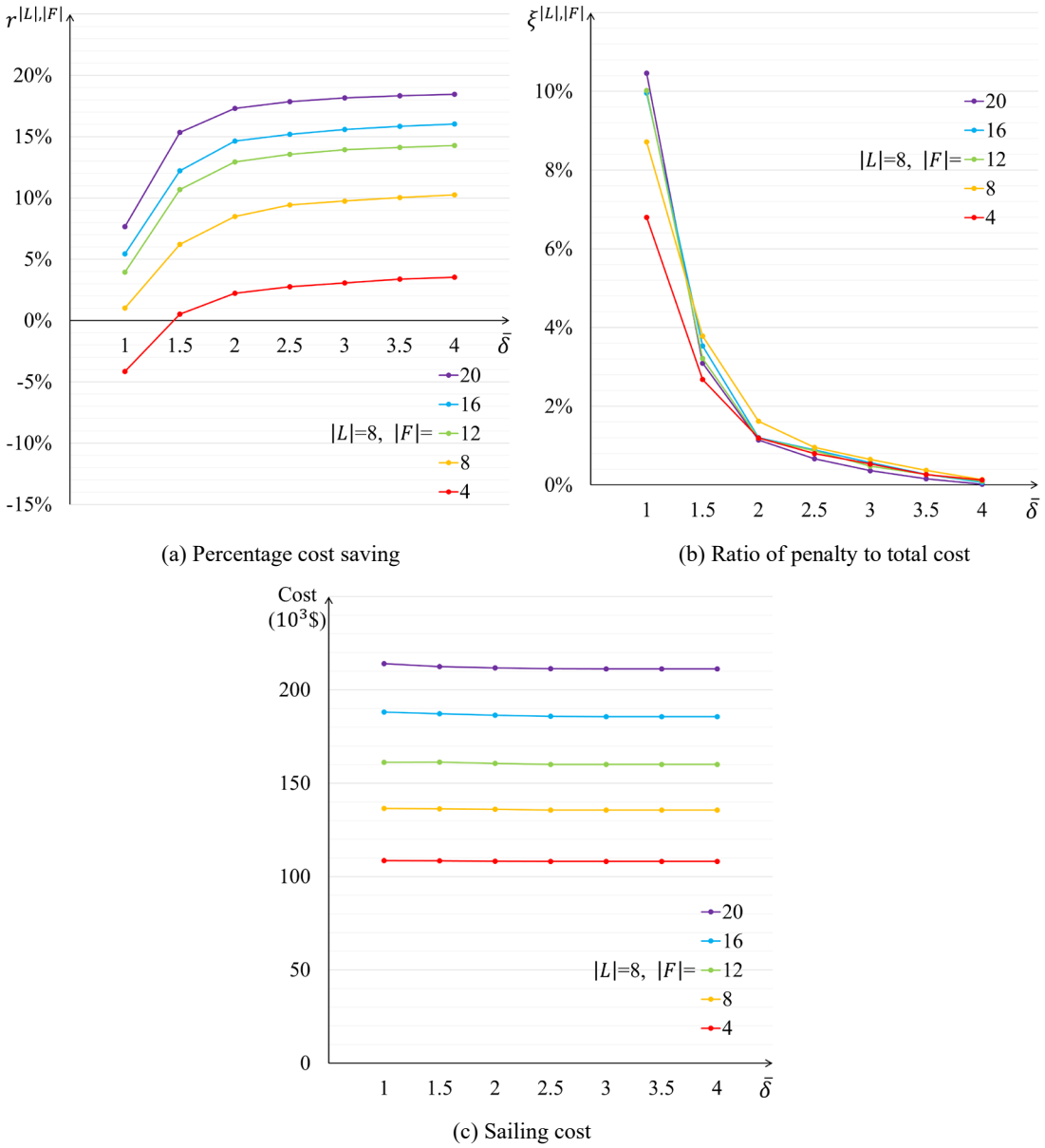

(a) Percentage cost saving

(b) Ratio of penalty to total cost

(c) Sailing cost

Fig. 3.6. Percentage cost saving, share of penalty cost, and sailing cost against $\bar{\delta}$.

3.2.6. Sensitivity to the Vessel Train Size Limit

This section investigates the sensitivity of cost savings to the size limit $u_l = u$ ($\forall l \in L$). The $r^{|L|,|F|}$ and $\xi^{|L|,|F|}$, averaged across ten randomly generated instances, are plotted against $u \in \{4, 8, 12, 16, 20\}$ in Fig. 3.7a-b, respectively. For simplicity, we set

$|F| = 20$ and $|L| \in \{4, 8, 12, 16, 20\}$. Note that the case where $u = 4$, $|L| = 4$, and $|F| = 20$ is infeasible since each of the four leader vessels must pilot at least 5 followers on average to be able to accommodate all the 20 autonomous vessels. This case is therefore removed.

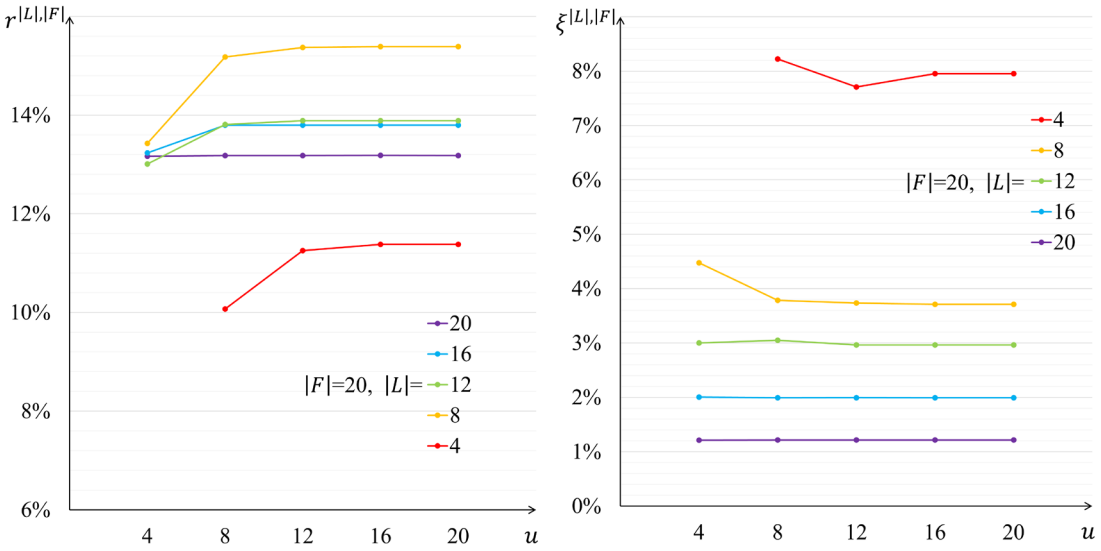

(a) Percentage cost saving (b) Ratio of penalty to total cost

Fig. 3.7. Percentage cost saving and share of penalty cost against u.

Fig. 3.7a shows for each value of $|L|$ that, as expected, the cost saving first grows with the size limit and then converges when u is sufficiently large (e.g., when $u \geq 4$ for $|L| = 20$, and $u \geq 8$ for $|L| = 12$ and 16). This means that vessel train operations can attain the maximum benefit with a limited threshold of vessel train size. Comparison across the different values of $|L|$ in Fig. 3.7a reveals that, when the number of autonomous ships is fixed, $r^{|L|,|F|}$ first increases and then decreases as $|L|$ grows (e.g., for $u \geq 8$, $r^{8,20} > r^{12,20} > r^{16,20} > r^{20,20} > r^{4,20}$). It first increases because more leader vessels can reduce the vessel train sizes and thus the detours and delays. However, when $|L|$ is sufficiently large (≥ 8), further increasing $|L|$ will undermine the

percentage cost saving since leader vessels are more expensive than autonomous ones. This finding implies that the benefit of vessel trains may peak at a certain ratio between the numbers of leader and follower vessels.

Fig. 3.7b reveals that the share of penalty cost is insensitive to u, except for a moderately larger share when $|L|$ and u are both small. In addition, the penalty share diminishes as $|L|$ increases, manifesting that more leader vessels can reduce the vessel delays due to the smaller vessel train sizes. Lastly, the sailing cost is again insensitive to u, and the results are omitted for brevity.

3.2.7. Sensitivity to the Network Topology

Our last batch of sensitivity analyses pertain to the effect of network topology on the cost saving of vessel trains. The network topology will affect the routing of vessel trains and the detour distances. An extreme case is where all the ports are located along a one-dimensional waterway and the hub port is located at the end of the waterway. This type of waterway network, despite its very simple topology, is common in the real world, for example, a river where the hub port is a sea port located at its estuary (Zhen et al. (2018)). The case is extreme because any vessel train dispatched from the hub port will take no detour during its journey. Thus, this type of topology represents an optimistic case for vessel train operations where the cost saving is maximized. In this section, we examine and compare the cost savings on this extreme type of waterway network against those on the Bohai Bay network.

Specifically, we consider a one-dimensional hypothetic network illustrated in Fig. 3.8. The network contains a hub port located at the left end of the river and eight feeder ports. For comparison, the distances between the feeder ports and the hub are set to the same values as in the Bohai Bay case. All the other parameters, including the OD pairs and the associated time windows, are set to the same values between the two networks.

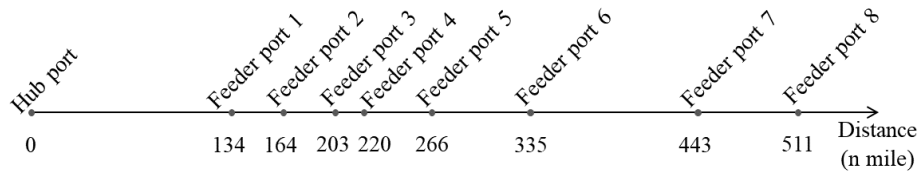

Fig. 3.8. Distances from the hub to the feeder ports in the one-dimensional hypothetic network.

We set $|L|, |F| \in \{4, 8, 12, 16, 20\}$ and calculate the $r^{|L|,|F|}$, $\xi^{|L|,|F|}$, and the sailing cost, averaged across ten randomly generated instances, for either network and each pair of $(|L|, |F|)$. The results are plotted against $|F|$ in Fig. 3.9a-d. The solid and dashed curves in these figures represent the Bohai Bay case and the one-dimensional network case, respectively.

Fig. 3.9a-b show that for both networks, the cost saving increases with $|F|$, which is as expected. Deploying eight leader vessels brings the highest cost savings in both networks. However, the performance of cases with four leader vessels differs largely between the two networks. For the Bohai Bay network, $|L| = 4$ renders the lowest cost savings due to the high costs of detours and delay penalty. On the other hand, for the one-dimensional network, $|L| = 4$ produces the second-highest cost savings among

$|L| \in \{4, 8, 12, 16, 20\}$. The minimum cost savings occur in the latter network with $|L| = 20$ because conventional ships are more costly.

Comparing Fig. 3.9a and b reveals that vessel trains operating in the one-dimensional network produce greater cost savings than in the Bohai Bay case. This is due to the elimination of detours and the significant delay reductions. As $|L|$ increases from 4 to 20, the gap between the two networks diminishes from 6-12% to 1-2%. This is because in a regular hub-and-spoke network (e.g., the Bohai Bay case), fewer leaders render longer vessel trains and thus more detours and vessel delays. Contrarily, when more leaders are available, vessel trains will take more direct routes with lower delays.

Fig. 3.9c confirms that the delay penalty is much smaller in the one-dimensional network. In addition, the share of penalty in the total cost decreases as $|L|$ grows in both networks, which is intuitive.

Regarding the sailing cost, Fig. 3.9d shows that it is approximately a linear increasing function of $|L|$ and $|F|$ in either network. The one-dimensional network renders lower sailing costs than the Bohai Bay case, but the gap between the two networks diminishes as $|L|$ grows.

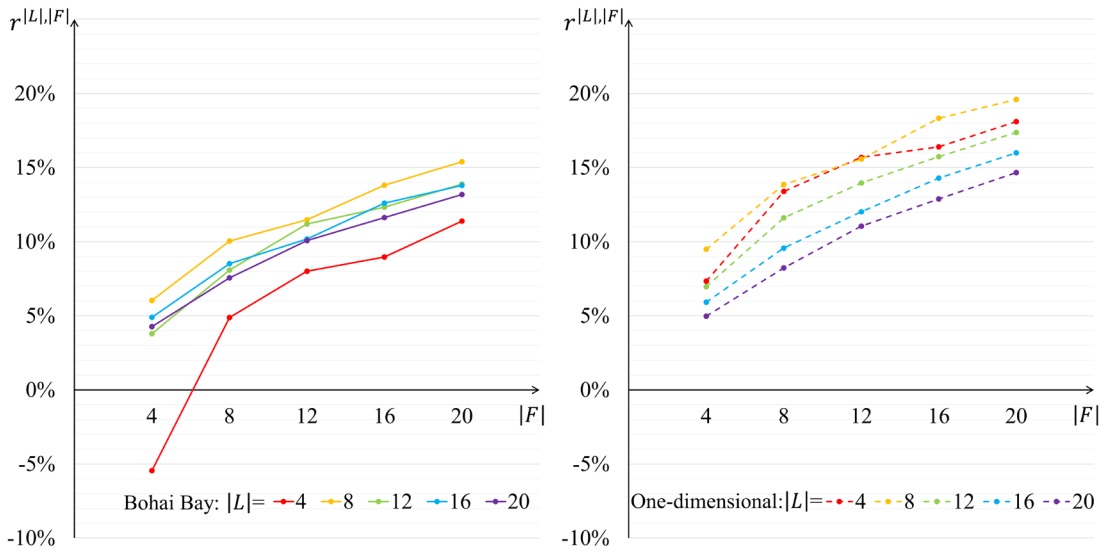

(a) Percentage cost saving for the Bohai Bay case (b) Percentage cost saving for the one-dimensional network

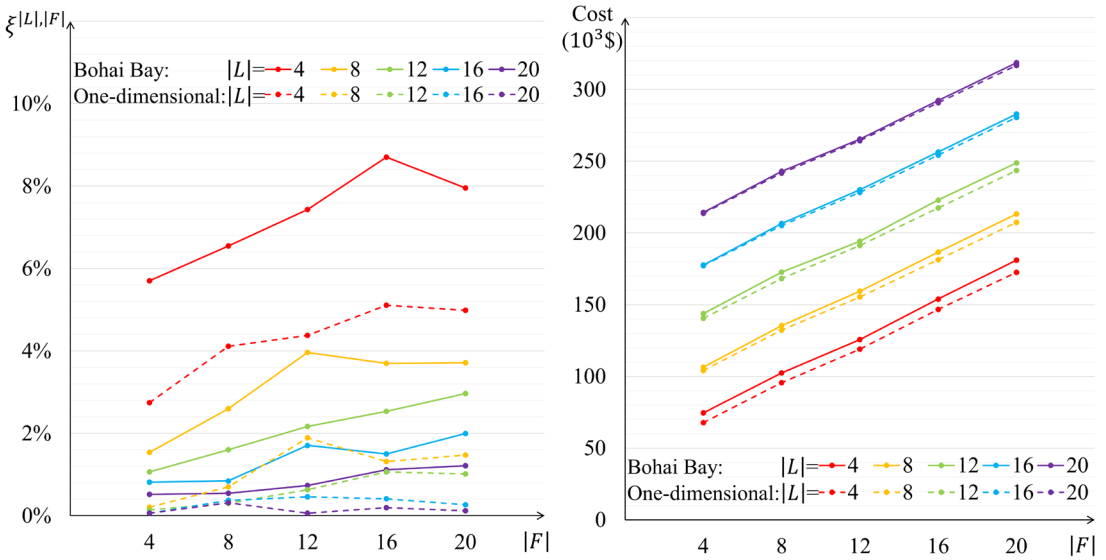

(c) Ratio of penalty to total cost (d) Sailing cost

Fig. 3.9. Percentage cost saving, share of penalty cost, and sailing cost for the two networks.

3.3. Summary

This chapter formulated the optimal scheduling of autonomous vessel trains for the freight distribution problem and the backhaul problem in hub-and-spoke networks. Novel nonlinear models were developed for minimizing the sum of vessel trains' sailing cost and lateness penalty by optimally assigning the autonomous follower vessels to the

leaders and determining the optimal departure time and the port calling sequence of each vessel train. The models were solved by CPLEX after linearization.

Computational performance tests show that, albeit the CPU runtimes soar as the problem size grows, a typical problem of a practical scale (e.g., with 9 ports, 10 leader vessels, and 50 autonomous vessels) can be solved in several minutes.

Extensive numerical experiments were conducted to examine the cost savings of vessel train operations in or near the Bohai Bay of China compared to a benchmark scenario with conventional ships only. Sensitivity analyses were performed to unveil the cause-and-effect relations between the cost savings and key operating factors, including the autonomous vessels' cost rate, numbers of leader and follower vessels, penalty cost rate, tightness of sailing time windows, vessel train size limit, and shipping network topology.

Findings from the numerical results can inform practitioners on implementing the autonomous vessel train strategy. First of all, the results manifest the great economical potential of autonomous vessels even though they must be piloted by manned ships. For example, when a conventional leader pilots 1-4 autonomous vessels on average, the strategy can save up to 18% of the cost if operating an autonomous vessel is 30% cheaper than a conventional one and 34% if that is 50% cheaper (see Fig. 3.4a). Even greater savings can be achieved when vessel trains are operated in a one-dimensional waterway network, e.g., the Yangtze River of China; see Section 3.2.7. This is because

the detours incurred by vessel train operations would be minimal. In addition, the strategy is more suitable for time-insensitive cargo, which has either a loose sailing time window or a lower penalty rate (Fig. 3.5a and 3.6a), also thanks to the lower detour and delay costs incurred.

On the other hand, increasing the maximum size of vessel trains would only improve the cost saving moderately (Fig. 3.7a). In fact, too few leader vessels would render longer vessel trains, more detours, and greater delays, which increase the cost. Our numerical results suggest that a sufficient number of leader vessels (eight in the Bohai Bay case study) should be used to attain the best performance of vessel trains (see Fig. 3.7a and 3.9a).

Chapter 4. Conclusions

Section 4.1 summarizes the contributions of this dissertation. Section 4.2 discusses some possible extensions of the current work.

4.1. Contributions

In this dissertation, we investigate two types of optimal scheduling problems of autonomous ships: the autonomous ship scheduling problem for voyages with a waterway bottleneck, and the autonomous vessel train scheduling problem in a hub-and-spoke network. Although various ship scheduling problems have long been studied in the literature, ship scheduling problems focused on autonomous ships are seldom examined. To advance the current research frontier and shed light on further research and real-world implementation in the realm of autonomous ships, we formulate and optimally solve the above two problems for minimizing the total costs of all the autonomous ships including sailing costs and tardiness penalties, considering different levels of autonomy.

For the optimal scheduling of autonomous vessels passing a waterway bottleneck, we develop a novel schedule optimization model. The model minimizes the sum of autonomous vessels' bunker cost and lateness penalty at destinations by selecting the optimal autonomous vessel schedules for passing a common bottleneck and the associated speed profiles, and incorporating the realistic, nonlinear relationship between bunker consumption and sailing speed. The nonlinear model is linearized via

two approximations. The first one linearizes the bunker consumption function using a piecewise linear lower bound, while the second converts the original model to a binary integer program by discretizing the time.

Numerical experiments show that the discrete-time approximation model produces better solutions with lower computational costs than the continuous-time, piecewise-linear approximation, especially for large-scale problems. Comparison between the continuous-time and the discrete-time models via extensive numerical experiments also shows that, even though the two approximate models yield similar objective values, they produce quite different schedules for individual autonomous vessels. Scrutinization unveils that the solution from the discrete-time model is more accurate than that of the continuous-time approximate model. Moreover, the discrete-time model is much faster than the continuous-time one for large-scale instances. The finding indicates that the piecewise linear approximation method's accuracy and computational efficiency are limited, especially for large-scale problems.

Numerical case studies are conducted for a real-world waterway bottleneck, the Three Gorges Dam lock. Results reveal how the optimal cost components and autonomous vessels' schedules and delays are affected by key operating parameters, including the fuel prices, delay penalty rates, and the tightness of sailing time windows. Comparison against two benchmark scheduling strategies (one with no vessel coordination and the other adopting a naïve coordination) manifests the sizeable benefit of optimal autonomous vessel scheduling. By comparing against the other two

coordination strategies, we show that the optimal autonomous vessel scheduling can significantly reduce the cost, especially the tardiness penalty when the sailing time windows are tight. However, when the sailing time windows are very loose, the improvement of optimal autonomous vessel scheduling is small. These insights can inform ship operation managers on better coordinating vessels' passage schedules at bottlenecks under various conditions.

For the optimal scheduling of autonomous vessel trains in a hub-and-spoke network, we study the scheduling of autonomous vessel trains for the freight distribution problem and the backhaul problem. An autonomous vessel train is formed by a conventional (manned) leader vessel and several autonomous follower vessels. The leader vessel will escort all the autonomous followers throughout their journeys. This strategy allows for safely operating autonomous vessels with limited autonomy level, thus expediting the replacement of conventional vessels with this more economical and environmentally friendly type of vessels.

Novel nonlinear models are developed for minimizing the sum of vessel trains' sailing cost and lateness penalty by optimally assigning the autonomous follower vessels to the leader vessels and determining the optimal departure time and the port calling sequence of each vessel train. The models can be solved by CPLEX after linearization. Two mixed-integer programming models are developed, one for the freight distribution problem and the other for the backhaul problem.

Computational performance tests show that a typical problem of a practical scale can usually be solved in several minutes. Thus, practitioners can readily use our models to generate optimal autonomous vessel train assignments and schedules for daily feeder service operations in inland waterway, sea-river, and short-sea networks.

Solutions to these models capture the optimal tradeoff between the added detour and delay costs of vessel trains and the lower sailing cost of autonomous ships. Numerical case studies are carried out for a real-world short-sea shipping network around the Bohai Bay of China. Results reveal sizeable cost savings of vessel train operations as compared to using conventional ships only. Results manifest the great economical potential for autonomous ships even though they must be piloted by conventional ships. And even greater savings can be achieved when vessel trains are operated in a single river. Sensitivity analyses are performed to unveil how the benefit of vessel trains is affected by key operating factors, e.g., the numbers of conventional and autonomous ships, the ratio between their costs, the maximum vessel train length, and the network topology.

This part of study is the first to jointly optimize the assignment of autonomous ships to vessel trains, the sequences of ports of call, and the schedules of vessel trains. The results show sizable economic benefits of this novel operating strategy, and how key operating factors affect the performance of vessel trains. We believe that our study will shed light on more advanced research on autonomous ship scheduling problems accounting for further technological and operational details. These research works will

motivate real-world implementations of autonomous ships during the transitional period toward full autonomy.

4.2. Future Work

This dissertation will be built upon to investigate the following potential extensions in the future:

For the autonomous ship scheduling problem with a waterway bottleneck, our models and results rely on certain assumptions, e.g., that a central operation manager can fully control all the autonomous vessel itineraries. This may occur when all these vessels belong to the same shipping company. Extension can be studied to consider the case where different autonomous vessels belong to different companies, each seeking to minimize its own cost. A formulation built upon a game theory framework would be desirable. In an extreme case where each autonomous vessel makes its own decision, the bottleneck operator (e.g., the dam traffic manager) can charge congestion tolls to the autonomous vessels (like the tolls in the roadway bottleneck models) to "coordinate" them in a limited way. Further complexities will arise when the autonomous vessels' travel times or bottleneck passage times are affected by external factors (e.g., the tidal level, water flow) and thus exhibit a certain level of stochasticity.

For the autonomous vessel train scheduling problem, we adopted distinct idealizations to simplify the modeling work. For example, we assumed a fixed sailing speed for all the vessels and a fixed sailing cost rate independent of the sailing speed.

In reality, a vessel's bunker cost is a function of its sailing speed (Wang and Meng, 2012), and a vessel train should be able to adjust its speed to meet the target delivery times. In addition, a more sophisticated scheduling model may also consider the transshipment of autonomous ships between different vessel trains and the deadheading problem of vessel trains.

Appendices

Appendix A. Notation of the Optimal Scheduling of Autonomous Vessels Passing a Waterway Bottleneck

Indices:

v, i, j autonomous vessels;

τ time coordinate in the discrete-time model;

Sets:

V set of autonomous vessels;

Ψ_{1v} set of all the possible arrival times of autonomous vessel v at the bottleneck in the discrete-time model;

Ψ_{2v} set of all the possible travel times of autonomous vessel v from entering the bottleneck to arriving at its destination port in the discrete-time model;

Parameters:

L_{1v} (n mile), distance from autonomous vessel v's origin port to the bottleneck;

L_{2v} (n mile), distance from the bottleneck to autonomous vessel v's destination port;

T_v^0 (h), autonomous vessel v's departure time from its origin port;

T_v (h), autonomous vessel v's expected arrival time at its destination port;

$P_v(y_v)$ ($), tardiness penalty of autonomous vessel v as a function of its arrival time at the destination, y_v;

β_v ($/h), tardiness penalty per hour of autonomous vessel v;

$f_v(s)$ (ton/n mile), bunker consumption rate of autonomous vessel v traveling at speed s;

a_v, b_v coefficients of the bunker consumption function, $a_v > 0$, $b_v > 1$;

s (knot), sailing speed (of autonomous vessel v);

$s_v^{\max}$ (knot), the maximum sailing speed of autonomous vessel v;

ω (h), transit time for a vessel to pass through the bottleneck;

H (h), the minimum headway between the passages of two consecutive vessels through the bottleneck;

h' number of time intervals representing the minimum headway between the passages of two consecutive vessels through the bottleneck in the discrete-time model;

α ($/ton), bunker fuel price;

Δt (h), unit time interval in the discrete-time model;

M a sufficiently large number;

ε ($), error bound of the objective function value;

$\bar{\varepsilon}$ (tons/n mile), error bound for each nautical mile traveled;

$Q_{1v}(\lambda_v)$ (ton/n mile), bunker consumption rate of autonomous vessel v for travel time λ_v from its origin to the bottleneck;

$Q_{2v}(\mu_v)$ (ton/n mile), bunker consumption rate of autonomous vessel v for travel time μ_v from the bottleneck to its destination;

$\overline{Q}_{1v}(\lambda_v)$ (ton/n mile), a piecewise-linear lower-bound of $Q_{1v}(\lambda_v)$;

$\overline{Q}_{2v}(\mu_v)$ (ton/n mile), a piecewise-linear lower-bound of $Q_{2v}(\mu_v)$;

$\theta_{1vk}, \gamma_{1vk}$ slopes and intercepts of the linear segments used to construct the approximate function $\overline{Q}_{1v}(\lambda_v)$, $k \in \{1,2,\dots,K_{1v}\}$;

$\theta_{2vk}, \gamma_{2vk}$ slopes and intercepts of the linear segments used to construct the approximate function $\overline{Q}_{2v}(\mu_v)$, $k \in \{1,2,\ldots.,K_{2v}\}$;

K_{1v} number of linear segments used to construct the approximate function $\overline{Q}_{1v}(\lambda_v)$;

K_{2v} number of linear segments used to construct the approximate function $\overline{Q}_{2v}(\mu_v)$;

$\lambda_v^{\min}$ (h), lower bound of autonomous vessel v's travel time from its origin to the bottleneck;

$\lambda_v^{\max}$ (h), upper bound of autonomous vessel v's travel time from its origin to the bottleneck;

$\mu_v^{\min}$ (h), lower bound of autonomous vessel v's travel time from the bottleneck to its destination;

$\mu_v^{\max}$ (h), upper bound of autonomous vessel v's travel time from the bottleneck to its destination;

$\tau_1^{\min}$ the minimum time coordinate of all the autonomous vessels' possible arrival times at the bottleneck in the discrete-time model;

$\tau_1^{\max}$ the maximum time coordinate of all the autonomous vessels' possible arrival times at the bottleneck in the discrete-time model;

Decision variables:

x_v (h), arrival time of autonomous vessel v at the bottleneck;

y_v (h), arrival time of autonomous vessel v at its destination port;

p_v (h), autonomous vessel v's delay at its destination port;

λ_v (h), autonomous vessel v's travel time from its origin to the bottleneck;

μ_v (h), autonomous vessel v's travel time from the bottleneck to its destination;

q_{1v} (ton/n mile), bunker consumption rate of autonomous vessel v from its origin to the bottleneck;

q_{2v} (ton/n mile), bunker consumption rate of autonomous vessel v from the bottleneck to its destination;

$x_{\tau v}$ binary variable that equals 1 if autonomous vessel v arrives at the bottleneck at τ, and 0 otherwise;

$\xi_{\tau v}$ binary variable that equals 1 if autonomous vessel v's travel time from entering the bottleneck to arriving at its destination port is τ, and 0 otherwise.

Appendix B. The Outer Approximation and its Computational Limitation

First, divide the objective error bound ε (\$) by the fuel price α and the total distance traveled by all the autonomous vessels. This yields the error bound for each nautical mile traveled, denoted by $\bar{\varepsilon}$ (tons/n mile):

$$\bar{\varepsilon} = \frac{\varepsilon}{\alpha} \times \frac{1}{\sum_{v \in V}(L_{1v}+L_{2v})}. \quad \text{(B1)}$$

In what follows, we derive piecewise linear approximations $\bar{Q}_{1v}(\lambda_v)$ and $\bar{Q}_{2v}(\mu_v)$ $(\forall v \in V)$ that satisfy:

$$|\bar{Q}_{1v}(\lambda_v) - Q_{1v}(\lambda_v)| \leq \bar{\varepsilon}, |\bar{Q}_{2v}(\mu_v) - Q_{2v}(\mu_v)| \leq \bar{\varepsilon}, \forall v \in V \quad \text{(B2)}$$

Note that $Q_{1v}(\lambda_v)$ and $Q_{2v}(\mu_v)$ represent the bunker consumption per nautical mile for autonomous vessel v's two sailing legs. Thus, Equation (B2) guarantees (theoretically) that the error in the bunker consumption cost is no greater than ε.

We next present an algorithm that generates a convex piecewise-linear function $\bar{Q}_{1v}(\lambda_v)$ with as few linear segments as possible. The algorithm for generating $\bar{Q}_{2v}(\mu_v)$ is similar and thus omitted for brevity.

The algorithm uses the first-order derivative of $Q_{1v}(\lambda_v)$ and the inverse of $Q_{1v}(\lambda_v)$. These are presented as follows:

$$Q'_{1v}(\lambda_v) = -a_v b_v {L_{1v}}^{b_v} (\lambda_v)^{-b_v-1}, \forall v \in V \tag{B3}$$

$$Q_{1v}^{-1}(q) = L_{1v}\left(\frac{q}{a_v}\right)^{-\frac{1}{b_v}}, \forall v \in V. \tag{B4}$$

Since $Q_{1v}(\lambda_v)$ is a monotonically decreasing function, its inverse function exists and is also a decreasing function. Thus, $0 < Q_{1v}(\lambda_v) \leq \bar{\varepsilon}$ if $\lambda_v \geq Q_{1v}^{-1}(\bar{\varepsilon})$. This condition means the approximation $\bar{Q}_{1v}(\lambda_v)$ can be set to zero when $\lambda_v \geq Q_{1v}^{-1}(\bar{\varepsilon})$; see Fig. B1.

The algorithm is illustrated in Fig. B1. We start from a point that is $\bar{\varepsilon}$ below curve $Q_{1v}(\lambda_v)$ at the left end of the feasible range of λ_v, denoted by (λ_v^1, Q_{1v}^1) in the figure. Draw a tangent line from that point to curve $Q_{1v}(\lambda_v)$. End this line segment when the error from $Q_{1v}(\lambda_v)$ increases to $\bar{\varepsilon}$ again, i.e., at point (λ_v^2, Q_{1v}^2) in the figure. This tangent line will be the first one in the set of linear approximation functions. Similarly, draw the second tangent line to $Q_{1v}(\lambda_v)$ from point (λ_v^2, Q_{1v}^2). Repeat this process until

$\lambda_v^k \geq \min\{Q_{1v}^{-1}(\bar{\varepsilon}), \lambda_v^{\max}\}$. If $\lambda_v^k < \lambda_v^{\max}$, add line $0 \cdot \lambda_v + 0$ to the set of linear approximation functions. Details of this algorithm are furnished below.

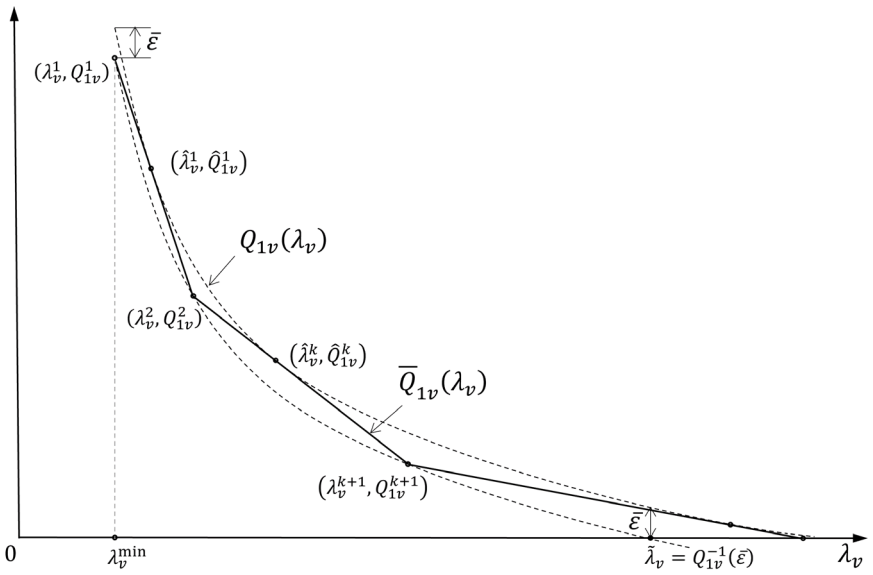

Fig. B1. Illustration of a piecewise linear approximation of $Q_{1v}(\lambda_v)$.

However, numerical errors arise in the above process, especially when solving Equation (B5) in Algorithm 1 for the point of tangency $(\hat{\lambda}_v^k, \hat{Q}_{1v}^k)$. Inspection of Fig. B1 reveals that the error would be relatively large under two conditions: (i) where the first-order derivative of the original bunker consumption function, $Q_{1v}'(\lambda_v)$, changes slowly, or equivalently, where $Q_{1v}''(\lambda_v)$ is small; and (ii) where the start point of the tangent line, (λ_v^k, Q_{1v}^k), is close to curve $Q_{1v}(\lambda_v)$. Unfortunately, both conditions are satisfied for our bunker consumption function. Condition (ii) becomes stronger when the predefined error bound ε is smaller. Moreover, the error in $(\hat{\lambda}_v^k, \hat{Q}_{1v}^k)$ would be amplified by the extrapolation for calculating $(\lambda_v^{k+1}, Q_{1v}^{k+1})$, the start of the next linear segment. Hence, the resulting approximation error may exceed the theoretical bound ε, and it may not

diminish as ε approaches zero. This could explain why the solution quality of [M2] does not match the expectation in Section 2.3.

Algorithm 1: Generate a piecewise linear approximation of $\boldsymbol{Q_{1v}(\lambda_v)}$ ($\boldsymbol{v \in V}$)

Step 0: Denote Ω the set of approximation lines. Initialize $\Omega = \emptyset$. Define $\lambda_v^{\min} = L_{1v}/s_v^{\max}$, $\tilde{\lambda}_v = Q_{1v}^{-1}(\bar{\varepsilon})$, and $\lambda_v^{\max}$ by (10a). Set $k = 1$, $\lambda_v^k = \lambda_v^{\min}$, and $Q_{1v}^k = Q_{1v}(\lambda_v^k) - \bar{\varepsilon}$.

Step 1: Add to Ω the line (numbered line k) that passes point (λ_v^k, Q_{1v}^k) and is tangential to $Q_{1v}(\lambda_v)$. The point of tangency, denoted by $(\hat{\lambda}_v^k, \hat{Q}_{1v}^k)$, can be obtained by solving the following equation for $\hat{\lambda}_v^k$ (and $\hat{Q}_{1v}^k = Q_{1v}(\hat{\lambda}_v^k)$):

$$Q'_{1v}(\hat{\lambda}_v^k) = \frac{Q_{1v}(\hat{\lambda}_v^k) - Q_{1v}^k}{\hat{\lambda}_v^k - \lambda_v^k}. \tag{B5}$$

Equation of line k is given by:

$$Q_{1v} - Q_{1v}^k = Q'_{1v}(\hat{\lambda}_v^k)(\lambda_v - \lambda_v^k). \tag{B6}$$

Set $\theta_{1vk} = Q'_{1v}(\hat{\lambda}_v^k)$ and $\gamma_{1vk} = Q_{1v}^k - Q'_{1v}(\hat{\lambda}_v^k)\lambda_v^k$. Then (B6) can be written as:

$$Q_{1v} = \theta_{1vk}\lambda_v + \gamma_{1vk}. \tag{B7}$$

Step 2: If the gap between line k and $Q_{1v}(\lambda_v)$ is not greater than $\bar{\varepsilon}$ when $\lambda_v = \min\{\tilde{\lambda}_v, \lambda_v^{\max}\}$, i.e.,

$$Q'_{1v}(\hat{\lambda}_v^k)\left(\min\{\tilde{\lambda}_v, \lambda_v^{\max}\} - \lambda_v^k\right) + Q_{1v}^k \geq Q_{1v}\left(\min\{\tilde{\lambda}_v, \lambda_v^{\max}\}\right) - \bar{\varepsilon}, \tag{B8}$$

go to Step 3.

Otherwise, there exists a unique point $(\lambda_v^{k+1}, Q_{1v}^{k+1})$ on line k, such that $\hat{\lambda}_v^k < \lambda_v^{k+1} < \min\{\tilde{\lambda}_v, \lambda_v^{\max}\}$ and $Q_{1v}^{k+1} = Q_{1v}(\lambda_v^{k+1}) - \bar{\varepsilon}$. The λ_v^{k+1} can be obtained by solving the following equation:

$$Q_{1v}(\lambda_v^{k+1}) - \bar{\varepsilon} - Q_{1v}^k = Q'_{1v}(\hat{\lambda}_v^k)(\lambda_v^{k+1} - \lambda_v^k). \tag{B9}$$

Set $k = k + 1$ and go to Step 1.

Step 3: Set $K_{1v} = k$. The $\overline{Q}_{1v}(\lambda_v)$ is defined by:

$$\overline{Q}_{1v}(\lambda_v) = \max\{0, \theta_{1vk}\lambda_v + \gamma_{1vk}, k = 1,2,\cdots,K_{1v}\}. \tag{B10}$$

Appendix C. Proof of Proposition 3

We first prove that (2.10a) is an upper bound of the optimal λ_v.

Denote $c_v(\lambda_v, \mu_v) = \alpha[L_{1v}Q_{1v}(\lambda_v) + L_{2v}Q_{2v}(\mu_v)] + \beta_v p_v$ the total bunker consumption and penalty cost for autonomous vessel $v \in V$. We next examine the value of λ_v that minimizes $c_v(\lambda_v, \mu_v)$. To this end, we consider that μ_v is fixed for now.

First, when $\lambda_v \leq -T_v^0 - \omega - \mu_v + T_v$, $p_v = 0$; see (2.4a) and (2.6e). In this case, $c_v(\lambda_v, \mu_v)$ is decreasing with λ_v because $Q_{1v}(\lambda_v)$ is a decreasing function of λ_v; see (2.7a).

On the other hand, when $\lambda_v > -T_v^0 - \omega - \mu_v + T_v$, $p_v = T_v^0 + \lambda_v + \omega + \mu_v - T_v$ which increases linearly with λ_v. Now $c_v(\lambda_v, \mu_v)$ becomes:

$$c_v(\lambda_v, \mu_v) = \alpha[L_{1v}Q_{1v}(\lambda_v) + L_{2v}Q_{2v}(\mu_v)] + \beta_v(T_v^0 + \lambda_v + \omega + \mu_v - T_v) \text{ , if } \lambda_v > -T_v^0 - \omega - \mu_v + T_v. \quad \text{(C1)}$$

The partial derivative of $c_v(\lambda_v, \mu_v)$ on λ_v is given by:

$$\frac{\partial c_v}{\partial \lambda_v} = \alpha L_{1v} Q'_{1v}(\lambda_v) + \beta_v = -\frac{\alpha a_v b_v {L_{1v}}^{b_v+1}}{(\lambda_v)^{b_v+1}} + \beta_v. \quad \text{(C2)}$$

Moreover, the second-order partial derivative of $c_v(\lambda_v, \mu_v)$ on λ_v is:

$$\frac{\partial^2 c_v}{\partial \lambda_v^2} = \frac{\alpha a_v b_v (b_v+1) {L_{1v}}^{b_v+1}}{(\lambda_v)^{b_v+2}} > 0 \quad \text{(C3)}$$

Thus, when $\lambda_v > -T_v^0 - \omega - \mu_v + T_v$ and μ_v is fixed, $c_v(\lambda_v, \mu_v)$ is convex with respect to λ_v and is minimized when $\frac{\partial c_v}{\partial \lambda_v} = 0$. This yields $\bar{\lambda}_v = L_{1v}\left(\frac{\alpha a_v b_v}{\beta_v}\right)^{\frac{1}{b_v+1}}$.

Combining the monotonically decreasing segment of $c_v(\lambda_v, \mu_v)$ when $\lambda_v \leq -T_v^0 - \omega - \mu_v + T_v$ and the convex segment when $\lambda_v > -T_v^0 - \omega - \mu_v + T_v$, we have:

$$\bar{\bar{\lambda}}_v = \max\left\{T_v - T_v^0 - \omega - \mu_v, L_{1v}\left(\frac{\alpha a_v b_v}{\beta_v}\right)^{\frac{1}{b_v+1}}\right\}. \quad \text{(C4)}$$

This is the value of λ_v that minimizes $c_v(\lambda_v, \mu_v)$ for a given μ_v. It is thus the optimal λ_v for autonomous vessel v if the interactions between autonomous vessels at the bottleneck are ignored and μ_v is given. Considering that $\mu_v \geq \frac{L_{2v}}{s_v^{\max}}$, any value of λ_v that is greater than the following bound will only increase autonomous vessel v's cost:

$$\bar{\bar{\lambda}}_v^{\max} = \max\left\{T_v - T_v^0 - \omega - \frac{L_{2v}}{s_v^{\max}}, L_{1v}\left(\frac{\alpha a_v b_v}{\beta_v}\right)^{\frac{1}{b_v+1}}\right\}. \quad \text{(C5)}$$

Now consider the interactions between autonomous vessels. Autonomous vessel v may not be able to pass the bottleneck at its own cost-minimizing time $\bar{\bar{\lambda}}_v$ (which is capped by $\bar{\bar{\lambda}}_v^{\max}$) because it may have to make way for other autonomous vessels. We consider a worst-case scenario, where the present autonomous vessel v must make way for all the other $|V| - 1$ autonomous vessels. Moreover, the other $|V| - 1$ autonomous vessels arrive at the bottleneck at $\bar{\bar{\lambda}}_v + H - \hat{\epsilon}$, $\bar{\bar{\lambda}}_v + 3H - 2\hat{\epsilon}$, $\bar{\bar{\lambda}}_v + 5H - 3\hat{\epsilon}$, …, $\bar{\bar{\lambda}}_v + (H - \hat{\epsilon}) + (2H - \hat{\epsilon})(|V| - 2)$, where $\hat{\epsilon}$ is a very small positive value. In this case, autonomous vessel v cannot pass the bottleneck between $\bar{\bar{\lambda}}_v$ and $\bar{\bar{\lambda}}_v + (2H - \hat{\epsilon})(|V| - 1)$ without delaying other autonomous vessels. In other words, it must pass the bottleneck either before $\bar{\bar{\lambda}}_v$ or after $\bar{\bar{\lambda}}_v + (2H - \hat{\epsilon})(|V| - 1)$. Since $\bar{\bar{\lambda}}_v + (2H -$

$\hat{\epsilon})(|V|-1) < \bar{\bar{\lambda}}_v + 2(|V|-1)H \le \bar{\bar{\lambda}}_v^{\max} + 2(|V|-1)H$, any value of λ_v greater than $\bar{\bar{\lambda}}_v^{\max} + 2(|V|-1)H$ will be suboptimal.

Finally, it is obvious that $\lambda_v^{\max} \ge \frac{L_{1v}}{s_v^{\max}}$. Combining the above results, we have:

$$\lambda_v^{\max} = \max\left\{\max\left\{T_v - T_v^0 - \omega - \frac{L_{2v}}{s_v^{\max}}, L_{1v}\left(\frac{\alpha a_v b_v}{\beta_v}\right)^{\frac{1}{b_v+1}}\right\} + 2(|V|-1)H, \frac{L_{1v}}{s_v^{\max}}\right\}, \forall v \in V, \quad \text{(C6)}$$

which is (2.10a).

Upper bound (2.10b) can be proved similarly. The only difference is that autonomous vessel v does not need to make way for other autonomous vessels after passing the bottleneck. Thus, term $2(|V|-1)H$ in (C6) will not appear in the upper bound of the optimal μ_v. □

Appendix D. First-come, First-serve Scheduling Strategy

The vessel scheduling solution and the associated cost under the FCFS strategy are formulated in three steps.

Step 1 minimizes each vessel v's schedule regardless of the minimum headway constraint. The model is denoted by [M4-v] for vessel $v \in V$:

[M4-v]

$$\min c(\lambda_v, \mu_v) = \alpha\left[L_{1v} a_v \left(\frac{L_{1v}}{\lambda_v}\right)^{b_v} + L_{2v} a_v \left(\frac{L_{2v}}{\mu_v}\right)^{b_v}\right] + \beta_v p_v \quad \text{(D1a)}$$

subject to

$$p_v = \max\{0, T_v^0 + \lambda_v + \omega + \mu_v - T_v\} \quad \text{(D1b)}$$

$$\lambda_v \geq \frac{L_{1v}}{s_v^{\max}} \tag{D1c}$$

$$\mu_v \geq \frac{L_{2v}}{s_v^{\max}}. \tag{D1d}$$

[M4-v] can be solved analytically. From the analysis in Appendix C, we know that for a fixed μ_v, the optimal λ_v is:

$$\lambda_v^*(\mu_v) = \max\left\{T_v - (T_v^0 + \omega + \mu_v), L_{1v}\left(\frac{\alpha a_v b_v}{\beta_v}\right)^{\frac{1}{b_v+1}}, \frac{L_{1v}}{s_v^{\max}}\right\}. \tag{D2}$$

For simplicity, we define $\tilde{\lambda}_v = \max\left\{L_{1v}\left(\frac{\alpha a_v b_v}{\beta_v}\right)^{\frac{1}{b_v+1}}, \frac{L_{1v}}{s_v^{\max}}\right\}$ and $\tilde{T}_v = T_v - (T_v^0 + \omega)$. Thus, $\lambda_v^*(\mu_v)$ is simplified as:

$$\lambda_v^*(\mu_v) = \max\{\tilde{T}_v - \mu_v, \tilde{\lambda}_v\}. \tag{D3a}$$

Note that if we swap λ_v with μ_v and L_{1v} with L_{2v} in (D1a-d), the formulation remains the same. Thus, we can similarly write the optimal μ_v as a function of λ_v:

$$\mu_v^*(\lambda_v) = \max\{\tilde{T}_v - \lambda_v, \tilde{\mu}_v\}. \tag{D3b}$$

where $\tilde{\mu}_v = \max\left\{L_{2v}\left(\frac{\alpha a_v b_v}{\beta_v}\right)^{\frac{1}{b_v+1}}, \frac{L_{2v}}{s_v^{\max}}\right\}$.

Combining (D3a-b), we consider the following two cases illustrated in Fig. D1a and b.

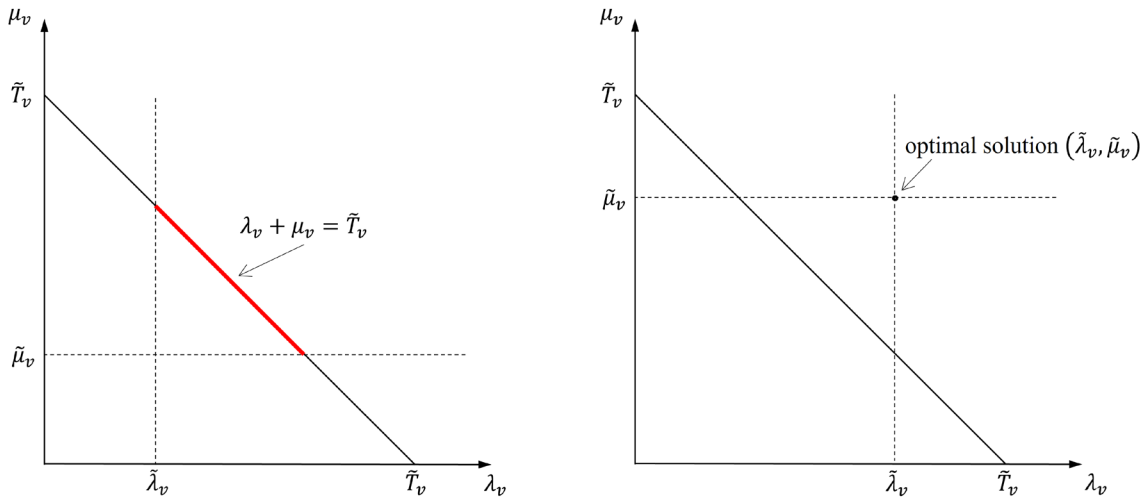

(a) when $\tilde{\lambda}_v + \tilde{\mu}_v \leq \tilde{T}_v$ (b) when $\tilde{\lambda}_v + \tilde{\mu}_v > \tilde{T}_v$

Fig. D1. Illustration of the two cases.

Case 1: when $\tilde{\lambda}_v + \tilde{\mu}_v \leq \tilde{T}_v$ (Fig. D1a). The reader can verify that the optimal solution of (λ_v, μ_v) satisfying (D3a-b) must lie in the red line segment in Fig. D1a, which is described by: $\lambda_v + \mu_v = \tilde{T}_v$, $\tilde{\lambda}_v \leq \lambda_v \leq \tilde{T}_v - \tilde{\mu}_v$. In this case, $p_v = 0$. Thus,

$$c(\lambda_v, \mu_v) \equiv \tilde{c}(\lambda_v) = \alpha a_v \left[L_{1v} \left(\frac{L_{1v}}{\lambda_v} \right)^{b_v} + L_{2v} \left(\frac{L_{2v}}{\tilde{T}_v - \lambda_v} \right)^{b_v} \right]. \tag{D4}$$

The first- and second-order derivatives of $\tilde{c}(\lambda_v)$ are:

$$\frac{d\tilde{c}}{d\lambda_v} = \alpha a_v \left[-b_v L_{1v}^{b_v+1} \lambda_v^{-b_v-1} + b_v L_{2v}^{b_v+1} \left(\tilde{T}_v - \lambda_v \right)^{-b_v-1} \right] \tag{D5}$$

$$\frac{d^2\tilde{c}}{d\lambda_v^2} = \alpha a_v \left[b_v(b_v+1) L_{1v}^{b_v+1} \lambda_v^{-b_v-2} + b_v(b_v+1) L_{2v}^{b_v+1} \left(\tilde{T}_v - \lambda_v \right)^{-b_v-2} \right] > 0. \tag{D6}$$

Thus, $\tilde{c}(\lambda_v)$ is a convex function, and its minimizer can be derived by letting $\frac{d\tilde{c}}{d\lambda_v} = 0$:

$$\hat{\lambda}_v = \frac{L_{1v} \tilde{T}_v}{L_{1v} + L_{2v}}. \tag{D7}$$

Considering the boundary constraint $\tilde{\lambda}_v \leq \lambda_v \leq \tilde{T}_v - \tilde{\mu}_v$, the optimal solution to (D1a-d) is:

$$\begin{cases} \lambda_v^* = \text{mid}\left(\tilde{\lambda}_v, \hat{\lambda}_v, \tilde{T}_v - \tilde{\mu}_v\right) \\ \mu_v^* = \tilde{T}_v - \lambda_v^* \end{cases}, \tag{D8}$$

where function $\text{mid}(\cdot)$ returns the middle one of the three arguments.

Case 2: when $\tilde{\lambda}_v + \tilde{\mu}_v > \tilde{T}_v$ (Fig. D1b). The reader can verify that there exists a unique optimal solution satisfying (D3a-b): $(\lambda_v^*, \mu_v^*) = \left(\tilde{\lambda}_v, \tilde{\mu}_v\right)$.

From the optimal solution (λ_v^*, μ_v^*), we derive the vessels' arrival time at the bottleneck, $\bar{x}_v = T_v^0 + \lambda_v^*, \forall v \in V$.

Step 2: Sort $\{\bar{x}_v, v \in V\}$ in ascending order. Denote the sorted sequence by $\{\bar{x}_{(i)}\}$, i.e., $\bar{x}_{(1)} \leq \bar{x}_{(2)} \leq \cdots \leq \bar{x}_{(|V|)}$. Incorporate constraints (2.2d) in the following way. Define a new sequence $\{\tilde{x}_{(i)}\}$ such that $\tilde{x}_{(1)} = \bar{x}_{(1)}$ and $\tilde{x}_{(i+1)} = \max\{\bar{x}_{(i+1)}, \tilde{x}_{(i)} + H\}$, $\forall i \in \{1,2, \dots, |V| - 1\}$. Note that $\{\bar{x}_v\}$ indicate the vessels' desired passage times while $\{\tilde{x}_{(i)}\}$ represent their actual passage times considering the minimum headway H.

Step 3: Given the updated vessel arrival times at the bottleneck, $\{\tilde{x}_{(i)}\}$, re-optimize μ_v for each vessel $v \in V$ using the following model denoted by [M5-v]:

[M5-v]

$$\min \alpha L_{2v} a_v \left(\frac{L_{2v}}{\mu_v}\right)^{b_v} + \beta_v p_v \tag{D9a}$$

subject to:

$$p_v = \max\{0, \tilde{x}_v + \omega + \mu_v - T_v\} \tag{D9b}$$

$$\mu_v \geq \frac{L_{2v}}{s_v^{\max}}. \tag{D9c}$$

where $\tilde{x}_v$ is obtained from $\{\tilde{x}_{(i)}\}$. [M5-v] can be simply solved using (D3b) by letting $\lambda_v = \tilde{x}_v - T_v^0$. Denote the optimal solution of [M5-v] by μ_v^{**} and the corresponding delay by p_v^{**}.

Given the above solution, calculate the total cost by: $\sum_{v\in V}\left\{\alpha\left[L_{1v}a_v\left(\frac{L_{1v}}{\lambda_v^*}\right)^{b_v} + L_{2v}a_v\left(\frac{L_{2v}}{\mu_v^{**}}\right)^{b_v}\right] + \beta_v p_v^{**}\right\}$. Note in the FCFS solution that $\tilde{x}_v$ is not always equal to $T_v^0 + \lambda_v^*$ ($v \in V$). When the two are not equal, the difference is vessel v's waiting time at the bottleneck.

Appendix E. Descending Penalty Scheduling Strategy

The vessel scheduling solution and the total cost under the DP strategy are also derived in three steps.

Step 1 is the same as Step 1 of the FCFS strategy (see Appendix D), which solves [M4-v] for each vessel $v \in V$ and calculates its arrival time at the bottleneck, $\bar{x}_v$.

Step 2: Adjust the vessel schedules in the descending penalty order to ensure constraints (2.2d) are satisfied.

Step 2.1: Sort the penalty rates $\{\beta_v, v \in V\}$ in descending order. Denote the resulting sequence by $\{\beta_{[i]}, i = 1,2,\dots,|V|\}$, i.e., $\beta_{[1]} \geq \beta_{[2]} \geq \cdots \geq \beta_{[|V|]}$. Write the corresponding sequence of $\bar{x}_v$ as $\{\bar{x}_{[i]}, i = 1,2,\dots,|V|\}$.

Step 2.2: Denote $\tilde{x}_{[i]}$ the actual arrival time of vessel $[i]$ at the bottleneck under the DP strategy. Initialize $\tilde{x}_{[i]} = \bar{x}_{[i]}$, $\forall i \in \{2,3,\dots,|V|\}$. Set $m = 2$.

Step 2.3: Find $l, n < m$ such that $l = \arg\max_{i<m}\{\tilde{x}_{[i]} | \tilde{x}_{[i]} \leq \tilde{x}_{[m]}\}$ and $n = \arg\min_{i<m}\{\tilde{x}_{[i]} | \tilde{x}_{[i]} \geq \tilde{x}_{[m]}\}$. Define $\Delta_1 = \tilde{x}_{[m]} - \tilde{x}_{[l]}$ and $\Delta_2 = \tilde{x}_{[n]} - \tilde{x}_{[m]}$. If l does not exist (i.e., $\tilde{x}_{[m]} < \tilde{x}_{[i]}, \forall i < m$), set $\Delta_1 = \infty$; and if n does not exist (i.e., $\tilde{x}_{[m]} > \tilde{x}_{[i]}, \forall i < m$), set $\Delta_2 = \infty$.

Step 2.4: Consider the following four cases regarding Δ_1 and Δ_2.

Case 1: $\Delta_1, \Delta_2 \geq H$. Set $m \leftarrow m + 1$. If $m > |V|$, go to Step 3. Otherwise, return to Step 2.3.

Case 2: $\Delta_1 < H$ and $\Delta_1 + \Delta_2 \geq 2H$. Set $\tilde{x}_{[m]} = \tilde{x}_{[l]} + H$. Set $m \leftarrow m + 1$. If $m > |V|$, go to Step 3. Otherwise, return to Step 2.3.

Case 3: $\Delta_1 < H$ and $\Delta_1 + \Delta_2 < 2H$. Set $\tilde{x}_{[m]} = \tilde{x}_{[n]} + H$. Return to Step 2.3.

Case 4: $\Delta_1 \geq H$ and $\Delta_2 < H$. Set $\tilde{x}_{[m]} = \tilde{x}_{[n]} + H$. Return to Step 2.3.

Step 3: Given the updated vessel arrival times at the bottleneck, $\{\tilde{x}_{[i]}\}$, re-optimize μ_v for each vessel $v \in V$ using [M5-v] in Appendix D. Calculate vessel v's arrival time $\tilde{y}_v$, $\forall v \in V$. Calculate the total cost under the DP strategy using (2.2a).

Under the DP strategy, the vessels experience no waiting time because the central operation manager will determine each vessel's speed profile and arrival time at the bottleneck.

Appendix F. Notation of the Optimal Scheduling of Autonomous Vessel Trains in a Hub-and-Spoke Network

Indices:

i, j	indices of ports, $i, j \in P$, $i = 0$ indicates the hub port;
l	index of a leader ship or a vessel train led by ship l, $l \in L$;
f, k	indices of autonomous follower ships, $f, k \in F$;

Sets:

P	set of all the ports, $P \equiv \{0, 1, \ldots, \lvert P \rvert\}$;
L	set of all the conventional leader ships, $L \equiv \{1,2, \cdots, \lvert L \rvert\}$;
F	set of all the autonomous follower ships, $F \equiv \{\lvert L \rvert + 1, \cdots, \lvert L \rvert + \lvert F \rvert\}$;

Parameters:

$t_{i,j}$	direct travel time from port i to port j, $t_{i,j} = t_{j,i}$, $t_{i,i} = 0$, $i, j \in P$;
d_l, d_f	destination port of leader ship $l \in L$ or follower ship $f \in F$;
T_l, T_f	the earliest departure time of leader ship $l \in L$ or follower ship $f \in F$ from the hub port;
T_l', T_f'	the latest expected arrival time of leader ship $l \in L$ or follower ship $f \in F$ at its destination port;
c_l, c_f	sailing cost rate of leader ship $l \in L$ or follower ship $f \in F$ per unit travel time;
p_l, p_f	penalty cost rate for leader ship $l \in L$ or follower ship $f \in F$ per unit delay at its destination port;
u_l	the maximum number of follower ships that can be led by $l \in L$;
M	a sufficiently large number;

Decision variables:

$\phi_{l,f}$ binary variable that equals 1 if $l \in L$ is the leader of $f \in F$, and 0 otherwise;

$\beta_{k,f}^{l}$ binary variable that equals 1 if, in vessel train $l \in L$, $f \in F$ arrives at its destination port next to $k \in F$, and 0 otherwise;

τ_l actual departure time of leader ship or vessel train $l \in L$ from the hub port;

τ_f actual departure time of follower ship $f \in F$ from the hub port;

λ_l, λ_f actual travel time of leader ship/vessel train $l \in L$ or follower ship $f \in F$;

Auxiliary variables:

θ_l, θ_f tardiness of leader ship $l \in L$ or follower ship $f \in F$.

References

Ahvenjärvi, S., 2016. The human element and autonomous ships. *TransNav: International Journal on Marine Navigation and Safety of Sea Transportation*, 10(3), 517–521.

Akbar, A., Aasen, A. K. A., Msakni, M. K., Fagerholt, K., Lindstad, E., Meisel, F., 2021. An economic analysis of introducing autonomous ships in a short-sea liner shipping network. *International Transactions in Operational Research*, 28(4), 1740–1764.

Arnott, R., de Palma, A., Lindsey, R., 1990. Economics of a bottleneck. *Journal of Urban Economics*, 27(1), 111–130.

Arnott, R., de Palma, A., Lindsey, R., 1993. A structural model of peak-period congestion: A traffic bottleneck with elastic demand. *The American Economic Review*, 83(1), 161–179.

Bhoopalam, A. K., Agatz, N., Zuidwijk, R., 2018. Planning of truck platoons: A literature review and directions for future research. *Transportation research. Part B: Methodological*, 107, 212–228.

Burmeister, H.-C., Rødseth, Ø. J., 2016. Maritime Unmanned Navigation through Intelligence in Networks. Available: http://www.unmanned-ship.org/munin/ [Accessed January 10, 2022].

Chen, L., Haseltalab, A., Garofano, V., Negenborn, R. R., 2019. Eco-VTF: Fuel-efficient vessel train formations for all-electric autonomous ships. *2019 18th European Control Conference (ECC)*. IEEE.

Chen, L., Huang, Y., Zheng, H., Hopman, H., Negenborn, R., 2020. Cooperative multi-vessel systems in urban waterway networks. *IEEE Transactions on Intelligent Transportation Systems*, 21(8), 3294–3307.

Christiansen, M., Fagerholt, K., Nygreen, B., Ronen, D., 2013. Ship routing and scheduling in the new millennium. *European Journal of Operational Research*, 228(3), 467–483.

Christiansen, M., Fagerholt, K., Ronen, D., 2004. Ship routing and scheduling: Status and perspectives. *Transportation Science*, 38(1), 1–18.

Colling, A., Hekkenberg, R., 2020. Waterborne platooning in the short sea shipping sector. *Transportation Research Part C: Emerging Technologies*, 120, 102778.

Connolly, M., 2021. Panama Canal delays near 10 days. Available: https://www.argusmedia.com/en/news/2203100-panama-canal-delays-near-10-days [Accessed November 1, 2021].

de Palma, A., Ben-Akiva, M., Lefevre, C., Litinas, N., 1983. Stochastic equilibrium model of peak period traffic congestion. *Transportation Science*, 17(4), 430–453.

Deng, Y., Sheng, D., Liu, B., 2021. Managing ship lock congestion in an inland waterway: A bottleneck model with a service time window. *Transport Policy*, 112, 142–161.

Escario, J. B., Jimenez, J. F., Giron-Sierra, J. M., 2012. Optimisation of autonomous ship manoeuvres applying Ant Colony Optimisation metaheuristic. *Expert Systems with Applications*, 39(11), 10120–10139.

Ghaderi, H., 2019. Autonomous technologies in short sea shipping: Trends, feasibility and implications. *Transport Reviews*, 39(1), 152–173.

Goel, A., 2010. Truck driver scheduling in the European Union. *Transportation Science*, 44(4), 429–441.

Goel, A., 2014. Hours of service regulations in the United States and the 2013 rule change. *Transport Policy*, 33, 48–55.

Goel, A., Archetti, C., Savelsbergh, M., 2012. Truck driver scheduling in Australia. *Computers & Operations Research*, 39(5), 1122–1132.

Golias, M. M., Saharidis, G. K., Boile, M., Theofanis, S., Ierapetritou, M. G., 2009. The berth allocation problem: Optimizing vessel arrival time. *Maritime Economics & Logistics*, 11(4), 358–377.

Gu, Y., Goez, J. C., Guajardo, M., Wallace, S. W., 2020. Autonomous vessels: State of the art and potential opportunities in logistics. *International Transactions in Operational Research*, 28(4), 1706–1739.

Han, X., Ma, R., Zhang, H. M., 2020. Energy-aware trajectory optimization of CAV platoons through a signalized intersection. *Transportation Research Part C: Emerging Technologies*, 118, 102652.

Hermans, J., 2014. Optimization of inland shipping: A polynomial time algorithm for the single-ship single-lock optimization problem. *Journal of Scheduling*, 17(4), 305–319.

Höyhtyä, M., Huusko, J., Kiviranta, M., Solberg, K., Rokka, J., 2017. Connectivity for autonomous ships: Architecture, use cases, and research challenges. *2017 International Conference on Information and Communication Technology Convergence (ICTC)*. IEEE.

Im, I., Shin, D., Jeong, J., 2018. Components for smart autonomous ship architecture based on intelligent information technology. *Procedia Computer Science*, 134, 91–98.

Kalouptsidi, M., 2021. The role of shipping in world trade. Available: https://econofact.org/the-role-of-shipping-in-world-trade [Accessed January 27, 2022].

Karlis, T., 2018. Maritime law issues related to the operation of unmanned autonomous cargo ships. *WMU Journal of Maritime Affairs*, 17(1), 119–128.

Khare, N., Singh, P., 2012. Modeling and optimization of a hybrid power system for an unmanned surface vehicle. *Journal of Power Sources*, 198, 368–377.

Klein, N., Guilfoyle, D., Karim, M. S., McLaughlin, R., 2020. Maritime autonomous vehicles: New frontiers in the law of the sea. *The International & Comparative Law Quarterly*, 69(3), 719–734.

Kremer, J., 2021. News and media Yara Birkeland. Available: https://www.yara.com/news-and-media/press-kits/yara-birkeland-press-kit/ [Accessed January 10, 2022].

Kretschmann, L., Burmeister, H.-C., Jahn, C., 2017. Analyzing the economic benefit of unmanned autonomous ships: An exploratory cost-comparison between an autonomous and a conventional bulk carrier. *Research in Transportation Business & Management*, 25, 76–86.

Laih, C.-H., Sun, P.-Y., 2014. The optimal toll scheme for ships queuing at the entrance of Panama Canal. *Maritime Economics & Logistics*, 16(1), 20–32.

Laih, C.-H., Tsai, Y.-C., Chen, Z.-B., 2015. Optimal non-queuing pricing for the Suez Canal. *Maritime Economics & Logistics*, 17(3), 359–370.

Lalla-Ruiz, E., Shi, X., Voß, S., 2018. The waterway ship scheduling problem. *Transportation Research Part D: Transport and Environment*, 60, 191–209.

LaRocco, L. A., 2021. Suez Canal blockage is delaying an estimated $400 million an hour in goods. Available: https://www.cnbc.com/2021/03/25/suez-canal-blockage-is-delaying-an-estimated-400-million-an-hour-in-goods.html [Accessed November 1, 2021].

Lave, L. B., DeSalvo, J. S., 1968. Congestion, tolls, and the economic capacity of a waterway. *Journal of Political Economy*, 76(3), 375–391.

Lesch, V., Breitbach, M., Segata, M., Becker, C., Kounev, S., Krupitzer, C., 2021. An overview on approaches for coordination of platoons. *IEEE Transactions on Intelligent Transportation Systems*, in press.

Li, Z.-C., Lam, W. H. K., Wong, S. C., 2017. Step tolling in an activity-based bottleneck model. *Transportation Research Part B: Methodological*, 101, 306–334.

Liang, X., Zhang, Y., Yang, G., 2021. Platoon control design for unmanned surface vehicles subject to input delay. *Scientific Reports*, 11(1), 1481.

Liu, Z., Zhang, Y., Yu, X., Yuan, C., 2016. Unmanned surface vehicles: An overview of developments and challenges. *Annual Reviews in Control*, 41, 71–93.

Meersman, H., Moschouli, E., NanwayBoukani, L., Sys, C., van Hassel, E., Vanelslander, T., Van de Voorde, E., 2020. Evaluating the performance of the vessel train concept. *European Transport Research Review*, 12(1), 1–11.

Meisel, F., Fagerholt, K., 2019. Scheduling two-way ship traffic for the Kiel Canal: Model, extensions and a matheuristic. *Computers & Operations Research*, 106, 119–132.

Meng, Q., Wang, S., Andersson, H., Thun, K., 2014. Containership routing and scheduling in liner shipping: Overview and future research directions. *Transportation Science*, 48(2), 265–280.

Meng, Q., Wang, S., Lee, C.-Y., 2015. A tailored branch-and-price approach for a joint tramp ship routing and bunkering problem. *Transportation Research Part B: Methodological*, 72, 1–19.

Miller, G., 2020. How the Panama Canal traffic jam is affecting ocean shipping. Available: https://www.freightwaves.com/news/how-the-panama-canal-traffic-jam-is-affecting-ocean-shipping [Accessed November 1, 2021].

Munim, Z. H., 2019. Autonomous ships: A review, innovative applications and future maritime business models. *Supply Chain Forum: An International Journal*, 20(4), 266–279.

Naeem, W., Xu, T., Sutton, R., Tiano, A., 2008. The design of a navigation, guidance, and control system for an unmanned surface vehicle for environmental monitoring. *Proceedings of the Institution of Mechanical Engineers, Part M: Journal of Engineering for the Maritime Environment*, 222(2), 67–79.

NGDCNH, 2009. *Marine Distance Tables for China Coast*. The Navigation Guarantee Department of The Chinese Navy Headquarters. China Navigation Publication Press.

Notteboom, T. E., 2006. The time factor in liner shipping services. *Maritime Economics & Logistics*, 8(1), 19–39.

Passchyn, W., Coene, S., Briskorn, D., Hurink, J. L., Spieksma, F. C. R., Vanden Berghe, G., 2016. The lockmaster's problem. *European Journal of Operational Research*, 251(2), 432–441.

Pomfret, R., 2019. The Eurasian Land Bridge: Linking regional value chains along the New Silk Road. *Cambridge Journal of Regions, Economy & Society*, 12(1), 45–56.

Psaraftis, H. N., 2019. Ship routing and scheduling: The cart before the horse conjecture. *Maritime Economics & Logistics*, 21(1), 111–124.

Rødseth, Ø. J., 2017. From concept to reality: Unmanned merchant ship research in Norway. *2017 IEEE Underwater Technology (UT)*. IEEE.

Rogers, H., 2018. Panama Canal and LNG: Congestion Ahead? Available: https://www.oxfordenergy.org/wpcms/wp-content/uploads/2018/04/Panama-Canal-and-LNG-%E2%80%93-Congestion-Ahead-Insight-33.pdf [Accessed November 1, 2021].

Ronen, D., 1983. Cargo ships routing and scheduling: Survey of models and problems. *European Journal of Operational Research*, 12(2), 119–126.

Ronen, D., 1993. Ship scheduling: The last decade. *European Journal of Operational Research*, 71(3), 325–333.

Ronen, D., 2011. The effect of oil price on containership speed and fleet size. *Journal of the Operational Research Society*, 62(1), 211–216.

Rusinov, I., Gavrilova, I., Sergeev, M., 2021. Features of sea freight through the Suez Canal. *Transportation Research Procedia*, 54, 719–725.

Sala, M., Soriguera, F., 2021. Capacity of a freeway lane with platoons of autonomous vehicles mixed with regular traffic. *Transportation Research Part B: Methodological*, 147, 116–131.

Ship and Bunker, 2021. Singapore Bunker Prices. Available: https://shipandbunker.com/prices/apac/sea/sg-sin-singapore [Accessed November 1, 2021].

Sina News, 2020. It takes three hours to pass the lock of the Three Gorges Dam, so where is the time spent! Available: http://k.sina.com.cn/article_6427581697_m17f1d1d0100100qtis.html?sudaref=www.baidu.com&display=0&retcode=0 [Accessed November 1, 2021].

Small, K. A., 2015. The bottleneck model: An assessment and interpretation. *Economics of Transportation*, 4(1), 110–117.

Tan, Z., Wang, Y., Meng, Q., Liu, Z., 2018. Joint ship schedule design and sailing speed optimization for a single inland shipping service with uncertain dam transit time. *Transportation Science*, 52(6), 1570–1588.

Tsugawa, S., Jeschke, S., Shladover, S. E., 2016. A review of truck platooning projects for energy savings. *IEEE Transactions on Intelligent Vehicles*, 1(1), 68–77.

Tvete, H. A., 2022. The ReVolt – A new inspirational ship concept. Available: https://www.dnv.com/technology-innovation/revolt/ [Accessed January 10, 2022].

UNCTAD, 2020. Review of Maritime Transport 2020. United Nations Conference on Trade and Development. Available: https://unctad.org/system/files/official-document/rmt2020_en.pdf [Accessed November 1, 2021].

UNCTAD, 2021a. Global Trade Update November 2021. United Nations Conference on Trade and Development. Available: https://unctad.org/system/files/official-document/ditcinf2021d4_en.pdf [Accessed January 27, 2022].

UNCTAD, 2021b. Review of Maritime Transport 2021. United Nations Conference on Trade and Development. Available: https://unctad.org/system/files/official-document/rmt2021_en_0.pdf [Accessed January 27, 2022].

Van Brummelen, J., O'Brien, M., Gruyer, D., Najjaran, H., 2018. Autonomous vehicle perception: The technology of today and tomorrow. *Transportation Research Part C: Emerging Technologies*, 89, 384–406.

Vickrey, W. S., 1969. Congestion theory and transport investment. *The American Economic Review*, 59(2), 251–260.

Wahlström, M., Hakulinen, J., Karvonen, H., Lindborg, I., 2015. Human factors challenges in unmanned ship operations – insights from other domains. *Procedia Manufacturing*, 3, 1038–1045.

Wang, S., Meng, Q., 2012. Sailing speed optimization for container ships in a liner shipping network. *Transportation Research Part E: Logistics and Transportation Review*, 48(3), 701–714.

Wang, S., Meng, Q., Liu, Z., 2013. Bunker consumption optimization methods in shipping: A critical review and extensions. *Transportation Research Part E: Logistics and Transportation Review*, 53, 49–62.

Wen, M., Ropke, S., Petersen, H. L., Larsen, R., Madsen, O. B. G., 2016. Full-shipload tramp ship routing and scheduling with variable speeds. *Computers & Operations Research*, 70, 1–8.

WTO, 2021. Global trade rebound beats expectations but marked by regional divergences. World Trade Organization. Available: https://www.wto.org/english/news_e/pres21_e/pr889_e.htm [Accessed November 26, 2021].

Wu, J., Ahn, S., Zhou, Y., Liu, P., Qu, X., 2021. The cooperative sorting strategy for connected and automated vehicle platoons. *Transportation Research Part C: Emerging Technologies*, 123, 102986.

Xiao, F., Zhang, H. M., 2013. Pareto-improving and self-sustainable pricing for the morning commute with nonidentical commuters. *Transportation Science*, 48(2), 159–169.

Yang, D., Jiang, L., Notteboom, T., 2019. Innovative solutions for shipping market turmoil: The search for profitability, sustainability and resilience. *Transport Policy*, 82, 75–76.

Yang, H., Meng, Q., 1998. Departure time, route choice and congestion toll in a queuing network with elastic demand. *Transportation Research Part B: Methodological*, 32(4), 247–260.

Zhang, L., Chen, F., Ma, X., Pan, X., 2020. Fuel economy in truck platooning: A literature overview and directions for future research. *Journal of Advanced Transportation*, 2020, 2604012.

Zhang, W., Wang, S., 2020. Autonomous vessel scheduling. *Journal of the Operations Research Society of China*, 8(3), 391–414.

Zhao, X., Lin, Q., Yu, H., 2020. A co-scheduling problem of ship lift and ship lock at the Three Gorges Dam. *IEEE Access*, 8, 132893–132910.

Zhen, L., Shen, T., Wang, S., Yu, S., 2016. Models on ship scheduling in transshipment hubs with considering bunker cost. *International Journal of Production Economics*, 173, 111–121.

Zhen, L., Wang, K., Wang, S., Qu, X., 2018. Tug scheduling for hinterland barge transport: A branch-and-price approach. *European Journal of Operational Research*, 265(1), 119–132.

Ziajka-Poznańska, E., Montewka, J., 2021. Costs and benefits of autonomous shipping – a literature review. *Applied Sciences*, 11(10), 4553.